Tilted outer and inner structures in edge-on galaxies?

Aleksandr V. Mosenkov [1,2]★ Anton A. Smirnov,[3,4] Olga K. Sil'chenko,[5]
R. Michael Rich [6] Vladimir P. Reshetnikov [3,7] and John Kormendy[8]

[1] *Informetrics Research Group, Ton Duc Thang University, Ho Chi Minh City, Vietnam*
[2] *Faculty of Applied Sciences, Ton Duc Thang University, Ho Chi Minh City, Vietnam*
[3] *St. Petersburg State University, 7/9 Universitetskaya nab., St. Petersburg 199034, Russia*
[4] *Central Astronomical Observatory at Pulkovo of RAS, Pulkovskoye Chaussee 65/1, 196140 St. Petersburg, Russia*
[5] *Sternberg Astronomical Institute of the Lomonosov Moscow State University, University Avenue 13, Moscow 119234, Russia*
[6] *Department of Physics & Astronomy, University of California Los Angeles, 430 Portola Plaza, Los Angeles, CA 90095-1547, USA*
[7] *Special Astrophysical Observatory, Russian Academy of Sciences, 369167 Nizhnij Arkhyz, Russia*
[8] *Department of Astronomy, University of Texas at Austin, 2515 Speedway, Mail Stop C1400, Austin, TX 78712, USA*

ABSTRACT
Tilted and warped discs inside tilted dark matter haloes are predicted from numerical and semi-analytical studies. In this paper, we use deep imaging to demonstrate the likely existence of tilted outer structures in real galaxies. We consider two SB0 edge-on galaxies, NGC 4469 and NGC 4452, which exhibit apparent tilted outer discs with respect to the inner structure. In NGC 4469, this structure has a boxy shape, inclined by $\Delta PA \approx 3°$ with respect to the inner disc, whereas NGC 4452 harbours a discy outer structure with $\Delta PA \approx 6°$. In spite of the different shapes, both structures have surface brightness profiles close to exponential and make a large contribution ($\sim$30 per cent) to the total galaxy luminosity. In the case of NGC 4452, we propose that its tilted disc likely originates from a former fast tidal encounter (probably with IC 3381). For NGC 4469, a plausible explanation may also be galaxy harassment, which resulted in a tilted or even a tumbling dark matter halo. A less likely possibility is accretion of gas-rich satellites several Gyr ago. New deep observations may potentially reveal more such galaxies with tilted outer structures, especially in clusters. We also consider galaxies, mentioned in the literature, where a central component (a bar or a bulge) is tilted with respect to the stellar disc. According to our numerical simulations, one of the plausible explanations of such observed 'tilts' of the bulge/bar is a projection effect due to a not exactly edge-on orientation of the galaxy coupled with a skew angle of the triaxial bulge/bar.

Key words: galaxies: evolution – galaxies: formation – galaxies: haloes – galaxies: interactions – galaxies: photometry – galaxies: structure.

1 INTRODUCTION

The structure of disc galaxies evolves by various internal (Kormendy & Kennicutt 2004; Kormendy 2013) and external (Kormendy & Bender 2012) processes. Galaxy discs can be flared, warped, tilted, and truncated (van der Kruit & Freeman 2011). All these prominent structural features can be explained by various evolution mechanisms, no one of which is universally dominant.

Galactic warps, seen as large-scale distortions of stellar and gaseous discs, when, starting at some radius, the tips of the outer isophotes start to bend, are very common in the Local Universe (Reshetnikov & Combes 1998) and were very frequent in the past (Reshetnikov et al. 2002). Optical observations show that at least 40–50 per cent of disc galaxies exhibit warps to some degree (Sanchez-Saavedra, Battaner & Florido 1990; Reshetnikov & Combes 1998; Ann & Park 2006; Ann & Bae 2016). Galactic warps are even more conspicuous in H I (Bosma 1981; Briggs 1990) and seen by H II regions (Paladini, Davies & De Zotti 2004;

Hou & Han 2014). The main proposed mechanisms to explain this phenomenon are misalignment between the disc and dark halo (Debattista & Sellwood 1999; Ideta et al. 2000), accretion on to the disc (Ostriker & Binney 1989; Jiang & Binney 1999; Shen & Sellwood 2006; Roškar et al. 2010), tidal interaction due to fast encounters (Vesperini & Weinberg 2000; Kormendy & Bender 2012; Kim et al. 2014; Semczuk et al. 2020), intergalactic magnetic fields (Battaner, Florido & Sanchez-Saavedra 1990; Battaner & Jimenez-Vicente 1998; Guijarro et al. 2010), and discrete bending modes (Sparke & Casertano 1988; Revaz & Pfenniger 2004).

Another important process, disc tilting, is a change of the overall angular momentum (vector) of the disc with time whereas disc warping implies that the direction of the angular momentum vector changes with galactocentric radius. In essence, disc tilting manifests itself as a slewing of the disc plane with time, with respect to its current orientation in the space. There are different processes which can cause galactic discs to tilt (see e.g. introduction in Earp et al. 2019): minor merging events (Ostriker & Tremaine 1975; Huang & Carlberg 1997; Kazantzidis et al. 2009; Bett & Frenk 2012), tumbling of dark matter haloes (Bailin & Steinmetz 2004;

★ E-mail: aleksandr.mosenkov@tdtu.edu.vn

Bryan & Cress 2007; DeBuhr, Ma & White 2012), and gas cooling on to the disc plane (Debattista et al. 2015; Earp et al. 2019). If a galaxy experiences an infall of a satellite, its disc also exhibits two other dynamical responses: warping and thickening (Huang & Carlberg 1997; Read et al. 2008; Kazantzidis et al. 2009; Sadoun, Mohayaee & Colin 2014). Tilting cannot be observed directly due to its extremely low tilting rate, even as compared to a typical galaxy rotation period ($\sim 5^{\circ}$ Gyr^{-1}, Bailin & Steinmetz 2004; Yurin & Springel 2015). However, the existence of some distinctive features in the disc structure, such as conspicuous S-shape warps or strong disc thickening may indirectly point to disc tilting or the result of a satellite accretion.

It was found that the angular momentum of the hot gas corona around galaxies, shock heated due to the falling of external gas into the dark matter's potential well, is usually misaligned with that of their stellar disc (van den Bosch et al. 2002; Roškar et al. 2010; Velliscig et al. 2015; Stevens et al. 2017). When the hot coronal gas cools, it settles into the disc (Fall & Efstathiou 1980; Kereš et al. 2005) and contributes misaligned angular momentum to the disc, which results in the disc tilting (Debattista et al. 2015; Earp et al. 2019). Consequently, it was found that the principal axes of dark matter haloes in blue star-forming galaxies are generally misaligned with the principal axes of their discs (Yang et al. 2006; Wang et al. 2008).

According to kinematic studies of nearby lenticular galaxies, misalignments between their stellar discs and gaseous components (from 40 per cent to 60 per cent of early-type galaxies have cool and ionized gas, Welch & Sage 2003; Sage & Welch 2006; Welch, Sage & Young 2010; Davis et al. 2011; Serra et al. 2012) are frequent (see e.g. Bertola, Buson & Zeilinger 1992; Kuijken, Fisher & Merrifield 1996; Sil'chenko & Moiseev 2006; Sil'chenko, Moiseev & Afanasiev 2009; Davis et al. 2011; Katkov, Moiseev & Sil'chenko 2011; Katkov, Sil'chenko & Afanasiev 2013; Katkov, Kniazev & Sil'chenko 2015; Proshina, Sil'chenko & Moiseev 2020). Davis et al. (2011) showed that misaligned gaseous subsystems are four times more frequent in field lenticular galaxies than in those residing in a cluster. Among strictly isolated nearby S0s, Katkov, Sil'chenko & Afanasiev (2014) found that half of all ionized-gas discs counterrotates the stars (see also Katkov et al. 2015). Recently, Sil'chenko, Moiseev & Egorov (2019) studied a sample of 18 S0 galaxies and found five galaxies with strongly inclined ionized gas discs. Some fraction of the gas observed in many S0s seems to be accreted in recent events, either due to tidal disruptions of massive gas-rich satellites (Kaviraj et al. 2009, 2011) or gas accretion from cosmological filaments (Thakar & Ryden 1996, 1998; Kereš et al. 2005; Dekel & Birnboim 2006).

Another interesting effect of disc tilting might be misalignment between inner and outer disc structures in edge-on galaxies. In this paper by inner and outer structures we mean that they are separated not only radially, but also vertically, so that an inner structure is enclosed in an outer structure. By tilting of a component we will call an observational effect where this component, as a whole, shows a different position angle than the general galaxy plane. Note here that we distinguish tilting from warping, which manifests itself in a vertical distortion of the disc starting at some radius, though both can have the same origin. The difference between disc warps and tilts is illustrated in Fig. 1. To this day, based on deep imaging, there has been no convincing observational evidence that the rather faint outer *stellar* structure in edge-on galaxies may exhibit tilting relative to the inner region in the sense that the inner and outer structures lie in different planes (see, however, our note below). Edge-on galaxies, as the best targets to study the vertical galaxy structure and disc tilting, were extensively studied in the optical and near-infrared (de
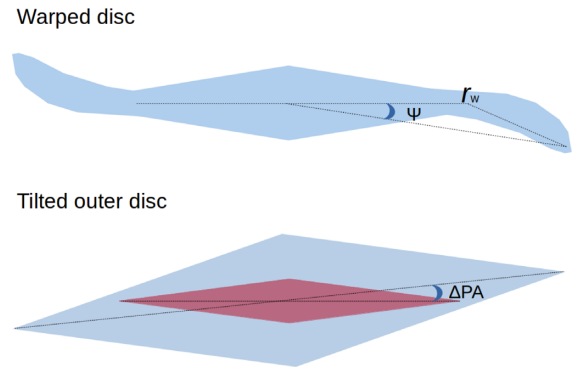

Figure 1. Difference between disc tilting and warping. The warp angle Ψ and the warp radius $r_{\rm W}$, where a warp starts, are also shown. The angle between the two different planes of the inner and outer discs in the bottom sketch is shown as ΔPA.

Grijs & van der Kruit 1996; Kregel, van der Kruit & de Grijs 2002; Mosenkov, Sotnikova & Reshetnikov 2010; Comerón et al. 2011; Martín-Navarro et al. 2012; Bizyaev et al. 2014; Ciambur & Graham 2016; Comerón, Salo & Knapen 2018), including deep observations (Martínez-Delgado et al. 2010; Miskolczi, Bomans & Dettmar 2011; Morales et al. 2018; Gilhuly et al. 2019; van Dokkum et al. 2019), but no systematic difference between the position angles in the inner and faint outer galaxy regions was noticed, except for Mosenkov et al. (2020) where they studied the outer shape of edge-on galaxies and found several galaxies with tilted outer isophotes. This paper is a follow-up study of Mosenkov et al. (2020).

In this paper, we consider a surface photometry of two SB0 galaxies with an apparent tilt of the outer structure with respect to the inner one as it represents a different disc which has a different position angle than the inner disc. NGC 4469 has been noted in Mosenkov et al. (2020), where they investigated deep imaging of 35 edge-on galaxies selected from the Halos and Environments of Nearby Galaxies (HERON) survey (Rich et al. 2019). We should note that M 82, the Cigar galaxy, which was also observed in the framework of the HERON survey, likewise shows tilted isophotes in the periphery (see Fig. 2), which may be associated with its spiral arms (Mayya, Carrasco & Luna 2005) or a disc warp (Notni & Bronkalla 1983). Also, this galaxy shows evident signs of interaction with its neighbour M 81 (Yun, Ho & Lo 1993). Taking into account the foregoing arguments and the peculiar nature of this well-known starburst galaxy (Rieke et al. 1980; Heckman, Armus & Miley 1990), we decided not to consider M 82 in our study. Another galaxy with a prominent tilted outer structure, NGC 509, which was classified by Mosenkov et al. (2020) as an edge-on galaxy, is in fact not so highly inclined, therefore we rejected it as well. In this study, we do not consider another remarkable edge-on galaxy from the HERON survey with an apparent tilt of the outer structure, NGC 4638, which exhibits a tilt of the bright stellar halo with respect to the disc. We are about to consider this galaxy among other edge-on galaxies with tilted bright haloes in our further paper, whereas in this study we mainly focus on tilted disc components. In addition to NGC 4469, NGC 4452 was chosen for this study incidentally, during a visual inspection of the EGIS catalogue of edge-on galaxies (Bizyaev et al. 2014). Using the technique described in Section 2 (see also Morales et al. 2018), we are likely to find more objects with such faint outer structures in our further studies.

Kormendy (1982) discussed isophote twists in non-edge-on galaxies which can be the result of tidal effects due to a close (or close in the past) companion. The best example is the spheroidal galaxy
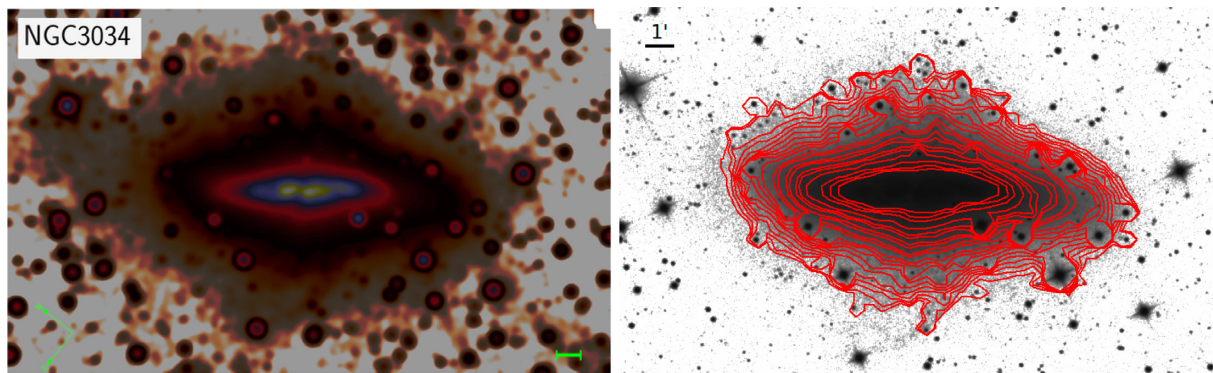
Figure 2. HERON image for NGC 3034 (left plot) and its superimposed isophotes from 20 to 26 mag arcsec^{-2} (right plot).

NGC 205 which exhibits an isophote twist towards M 31. Michard & Marchal ([1993](#)) (see also Michard & Marchal [1994](#)) found small twists of the isophotes for 10 nearly edge-on S0 galaxies, which are manifested in small trends in their major axis position angles and one of the Fourier harmonics responsible for the isophote asymmetry. They attributed this change of the position angle to a small difference of the major axis orientation between the central component (a bulge and/or bar) and an outer component (a disc or a halo). They estimate this tilt of a few degrees between the equatorial planes of these components, and claim that it is not associated with spiral arms and disc warps. Here we should note, however, that we revisited a photometry of these galaxies using the data preparation method described in Section 2 and established that all galaxies, except for NGC 4638, show either an inner twist of an inner triaxial structure (possibly, a bar) or 'a tilt' of the halo, but the estimated edge-on orientation of these galaxies is either questionable (e.g. NGC 2732 and NGC 7332) or not true (e.g. NGC 4036 and NGC 4251). It is evident that when there are triaxial components in a flat disc that has one tilt angle to the line of sight, then isophotes at different surface brightnesses will necessarily have different position angles. But how important this effect is when we consider almost edge-on galaxies? Do we observe edge-on galaxies with inner components with position angles that are different from that of the main disc? For a pedagogical purpose, in this paper we consider several not exactly edge-on galaxies (including NGC 509 in Appendix A) which exhibit tilting of the inner structure similar to those reported by Michard & Marchal ([1993](#)). We show that these structures may be, in fact, bars which appear tilted due to the projection effect.

This paper is organized as follows. In Section 2, we describe the data and image preparation for the two selected galaxies with possible titled outer discs. In Section 3, we consider in detail each of the selected galaxies. We discuss our results in Section 4 and make final conclusions in Section 5.

2 THE DATA

Here, we describe the data for NGC 4452 and NGC 4469, which we use in our photometric analysis in Section 3. For NGC 4469, its deep image has been considered in the framework of the HERON survey (Rich et al. [2019](#); Mosenkov et al. [2020](#)). However, here we analyse observations of both galaxies obtained from the Sloan Digital Sky Survey DR16 (SDSS; York et al. [2000](#); Ahumada et al. [2019](#)) and the DESI Legacy Imaging Surveys DR8 (hereafter Legacy, Dey et al. [2019](#)). This allows us to (1) explore the faint outer structure of these galaxies down to the same level of depth, and (2) study their colour maps. Also, the resolution in these surveys is better than

in the HERON survey, although their imaging is shallower (below, however, we describe how we increase their depth by stacking galaxy images in several optical wavebands, as proposed in Miskolczi et al. [2011](#) and Morales et al. [2018](#)). In principal, we could limit ourselves to use SDSS but Legacy has deeper imaging and a better resolution (see below), therefore we decided to use both data sources. Our image preparation is organized as follows.[1]

Using a special PYTHON script to download and concatenate adjacent fields from the SDSS archive,[2] we retrieve galaxy images for both galaxies in the *gri* bands (the *u* and *z* bands are rather shallow, Fukugita et al. [1996](#), so we do not use them) in an automated regime. Also, we download corresponding point spread function (PSF) images (extracted from the respective *psFields* files) in the same wavebands. These tiny images describe the core PSF (seeing), but for the wings of the scattered light we use an extended PSF from Infante-Sainz, Trujillo & Román ([2020](#)), which we rotate to align the drift scanning direction of the image with the drift scanning direction of the PSF. We then merge the inner (core) and outer (extended) PSFs by normalising them in an annulus 5 arcsec in width where the two PSFs overlap. After that, the galaxy images in the *g* and *i* bands are resampled to the *r* band using the created extended PSFs by means of PYPHER[3] package (Boucaud et al. [2016](#)) suited for PSF matching.

After that, for each galaxy image we create a segmentation map using SEXTRACTOR (Bertin & Arnouts [1996](#)) and increase the size of the regions of the general mask by a factor of two, to ensure that our mask covers all faint scattered light in the image. Then, we apply the created mask and fit the background with a first-order polynomial and subtract it from the initial image. Finally, we stack the galaxy images in all three bands – this increases the signal-to-noise ratio and, consequently, reduces the root-mean-square (rms) of the background. For this purpose we use the IRAF/INCOMBINE procedure. In the resultant image, we select good PSF (unsaturated) stars and measure the total fluxes of these stars using a procedure from the PYTHON package `photutils`. Then we cross-correlate the selected stars with the SDSS data base to retrieve their apparent magnitudes in the *r* band. By so doing, we are able to perform photometric calibration of the stacked image and estimate its zero-point in the *r* band. The procedure of stacking the three wavebands together allows us to improve the depth of the imaging by 1.1 mag, on average: 26.5 mag arcsec^{-2} for the individual bands versus 27.6 mag arcsec^{-2}

---

[1]It is realised with a dedicated PYTHON package IMAN https://bitbucket.org/mosenkov/iman_new.
[2]https://github.com/latrop/sdss_downloader.
[3]https://github.com/aboucaud/pypher.

for the stacked images, calculated at the 3σ level in a box of 10×10 arcsec^2 (we make use of this notation from Fliri & Trujillo [2016](#) throughout the paper).

In our final step, we mask out all objects which do not belong to the target galaxy. To do this, we use a special PYTHON script from the IMAN package which is based on the `mtobjects` tool[4] (Teeninga et al. [2015](#)): it effectively identifies all objects in an image and is robust for masking even in an automatic mode without a special tuning of input parameters.

The same pipeline is applied to the Legacy images in the *grz* bands, except that we do not do image resampling, as, at the moment, no extended PSFs have been produced for the Legacy imaging. We should note, however, that the image resampling is not a necessary step for enhancing the depth of the images and we only do this to be able to carry out photometric decomposition of the stacked SDSS galaxy images (see Section 3) using the matched PSFs. The image stacking of the Legacy data allows us to create final images with a depth of 28.3 mag arcsec^{-2} calibrated to the *r* band.

We also use observations in the NUV band from the Galaxy Evolution Explorer (GALEX; Martin et al. [2005](#); Bianchi, Conti & Shiao [2014](#)) and observations in the *W*1 band (3.4 μm) from the Wide-field Infrared Survey Explorer (*WISE*; Wright et al. [2010](#)) to estimate the NUV−*r* colour and the total stellar mass of the galaxies, respectively (see Section 3.2). The images were prepared using the above described routines except for image stacking.

3 ANALYSIS OF THE DATA

3.1 The methods

For each galaxy, we carry out an IRAF/ELLIPSE (Jedrzejewski [1987](#)) fit of the galaxy isophotes. We consider the distributions of the position angle PA, ellipticity $\epsilon = 1 - b/a$ (where a and b are the semimajor and semiminor axes, respectively) and the B_4 coefficient, which characterizes the shape of the isophotes, see below. Also, we provide a 2D photometric model, consisting of several structural components, using the IMFIT code (Erwin [2015](#)). We use its standard Levenberg–Marquardt algorithm for finding the optimal fit parameters. To estimate indicative uncertainties on our fit parameters, we vary the sky level using a set of Monte Carlo simulations (10 attempts) with the sky rms determined in Section 2. For uniformity, to fit the 2D intensity distribution for each structural component of the galaxies under study, we use a Sérsic function (Sérsic [1963](#), [1968](#)) with the following major-axis intensity profile

$$I(r) = I_e \exp \left\{ -b_n \left[\left(\frac{r}{r_e} \right)^{1/n} - 1 \right] \right\}, \quad (1)$$

where I_e is the surface brightness at the effective (half-light) radius r_e and n is the Sérsic index controlling the shape of the intensity profile. The function b_n is calculated via the polynomial approximation in Ciotti & Bertin ([1999](#)) (when $n > 0.36$) and MacArthur, Courteau & Holtzman ([2003](#)) (when $n \le 0.36$).

In our fits we consider generalized ellipses (Athanassoula et al. [1990](#); Erwin [2015](#)) with the following free parameters: position angle PA, ellipticity ϵ, and C_0, which controls the discy/boxy view of the isophote (when $C_0 < 0$ the isophotes look discy, whereas they become boxy if $C_0 > 0$ and $C_0 = 0$ if the isophotes can be represented by pure ellipses). Note that one of the output Fourier coefficients of the IRAF/ELLIPSE procedure, the B_4 coefficient, also characterizes

the discyness/boxyness of the isophotes, so that when $B_4 > 0$ the isophotes are discy and they look boxy if $B_4 < 0$. Apparently, there is a link between C_0 and B_4, but as they are derived using different approaches, the relation between them is not direct. Thus, we use both when needed.

We denote by *f* the fraction of light in a given component according to our models.

We should note here that we neglect the influence of dust on the estimated parameters of the photometric components. Although this assumption can be rather strong (as we can see below, NGC 4469 shows some traces of dust in the central galaxy region), the fraction of bolometric luminosity absorbed by dust in early-type (Hubble stage $T < 0.5$) galaxies is estimated to be 7.4 ± 0.8 per cent, on average, versus 24.9 ± 0.7 per cent for late-type ($T \ge 0.5$) galaxies (Bianchi et al. [2018](#)). Smith et al. ([2012](#)) also show that the stellar discs in S0s contain much less dust than the discs in late-type spirals.

3.2 General information on the galaxies

In Table [1](#), we list some general characteristics for both galaxies using their stacked images calibrated with the corresponding zero-points in the *r* band. We measured the total (asymptotic) magnitudes of the galaxies, along with the optical radii r_{25} at the isophote 25 mag arcsec^{-2}, using their curves of growth based on the performed IRAF/ELLIPSE fitting.

As one can see, both galaxies are classified as SB0. The two galaxies do not differ significantly in luminosity and represent quite modest by mass and size disc galaxies (see e.g. Shen et al. [2003](#)) with possible recent star formation: Kaviraj et al. ([2007](#)) showed that early-type galaxies with NUV−*r* < 5.5 might have experienced recent star formation (both NGC 4452 and NGC 4469 show colours close to this boundary value). However, NUV−*r* < 5.5 may also be related to the presence of evolved hot stars, the UV-upturn (Greggio & Renzini [1990](#)).

We also present the mean colours ($g - z$) for the inner region, outlined by an isophote of 24 mag arcsec^{-2}, and the outer region between the isophotes 24 mag arcsec^{-2} and 26 mag arcsec^{-2} (columns 9 and 10 in Table [1](#)). As one can see, the outer region is slightly bluer than the inner one for both galaxies, but this difference is insignificant.

3.3 Description of each galaxy

Below, we consider each of the selected galaxies in detail.

We compare the created deep images for NGC 4452 (SDSS and Legacy) and NGC 4469 (HERON, SDSS, and Legacy) and conclude that both galaxies show a tilted outer structure with respect to the inner one. Below we show the stacked images, isophote, and colour maps, as well as the results of the isophote analysis, based on the Legacy data. We use the stacked SDSS images to perform multicomponent decomposition, mainly to derive the parameters for the outer component, which is of great interest in this study. The HERON image for NGC 4469 can be found in fig. A1 in Mosenkov et al. ([2020](#)).

Both galaxies show the same difference between the total magnitude at the isophote 25 and 28 mag arcsec^{-2}, according to their curves of growth, as 0.09 mag, or an increase of 8.6 per cent of the flux within the optical radius.

3.3.1 NGC 4452

NGC 4452 is an SB0 edge-on galaxy close to the centre of the Virgo cluster. Kormendy & Bender ([2012](#)) classified it as S0c, according

---

[4] https://github.com/CarolineHaigh/mtobjects.

Table 1. Main parameters of the selected galaxies.

Galaxy	RA (J2000)	Dec. (J2000)	D (Mpc) (1)	Type (2)	r_{25} (arcmin) (3)	r_{25} (kpc) (4)	m_r (mag) (5)	M_r (mag) (6)	NUV$-r$ (mag) (7)	$\log M_*$ (M$_\odot$) (8)	$\langle g-z \rangle_o$ (mag) (9)	$\langle g-z \rangle_i$ (mag) (10)
NGC 4452	12:28:43	11:45:18	16.8	SB0	2.07	10.10	11.62	−19.51	5.32	9.95	1.15 ± 0.07	1.24 ± 0.16
NGC 4469	12:29:28	08:44:59	16.8	SB0-a	2.94	14.30	10.85	−20.28	5.49	10.46	1.29 ± 0.11	1.32 ± 0.34

Notes. Comuns: (1) Distance taken from the NASA/IPAC Extragalactic Database (NED) which is based on Tully & Fisher (1988) and calculated using the Tully–Fisher method (Tully & Fisher 1977). The method of surface brightness fluctuations (Tonry & Schneider 1988), applied by Mei et al. (2007) for 79 galaxies of the Virgo cluster, gives the mean distance $D = 16.5$ Mpc for 'all galaxies (no W' cloud)', which is close the distances adopted in this paper.
(2) Morphological type from HyperLeda,
(3) and (4) semi-major axis of the isophote 25 mag arcsec^{-2} in the *r* band,
(5) and (6) asymptotic magnitude in the *r* band taking into account the Galactic extinction from Schlafly & Finkbeiner (2011),
(7) colour based on the *GALEX* and SDSS photometry (corrected for the Galactic extinction but not corrected for the internal dust attenuation),
(8) total stellar mass computed from the galaxy luminosity in the *WISE W*1 band and using the prescriptions from Wen et al. (2013),
(9) mean colour for the region between the isophotes 24 and 26 mag arcsec^{-2} (corrected for the Galactic extinction but not corrected for the internal dust attenuation),
(10) mean colour for the region within the isophote 24 mag arcsec^{-2} (corrected for the Galactic extinction but not corrected for the internal dust attenuation).

to their updated van den Bergh's (van den Bergh 1976) parallel-sequence classification of galaxies. In Fig. 3, one can see an inner disc of high surface brightness with a sharp edge. The very thin inner structure gives us a hint that this galaxy is exactly edge-on or very close to it. The outer disc exhibits a remarkable tilt and warping increasing towards the periphery. Michard & Marchal (1994) observe a twist of the isophotes which they attribute to a warped thick disc as in NGC 4762. Sandage & Bedke (1994) and Kormendy & Bender (2012) also find NGC 4452 similar to NGC 4762. Our deep images do not reveal any interesting LSB features around NGC 4452.

In Fig. 4, one can see a steady increase of the position angle where the inner structure (disc or ring) is cut off: from $r \approx 37$ arcsec to the periphery the position angle changes up to $19°$. According to fig. 8 in Kormendy & Bender (2012), who used a high-resolution *HST* ACS F475W image to study the photometry of this galaxy in great detail, the inner structure is very flat ($\epsilon \gtrsim 0.9$), whereas due to the poor resolution of our stacked image the inner structure is smeared out and shows a lower flattening ($\epsilon \approx 0.77$). The advantage of this work is that we can study the galaxy out to very low surface brightness where the outer structure becomes very thick (up to $\epsilon \approx 0.5$ for $r \gtrsim 190$ arcsec in Fig. 4). The galaxy shows discy or oval isophotes at all radii ($B_4 \gtrsim 0$). Its outer structure is remarkably discy.

Ferrarese et al. (2006) find that there is no significant colour difference between the different components of the galaxy, except that its inner (nucleus) disc is bluer than the outer discs. Our lower resolution colour map in Fig. 5 shows that the inner structure is red whereas the colour distribution above and below the galaxy plane is slightly bluer. Also, we note a prominent colour gradient (see Fig. B1 in Appendix B): the galaxy is getting bluer at larger radii from the centre. Consolandi et al. (2016) studied radial profiles of galaxies in the Coma and Virgo superclusters and found that early-type galaxies show no colour gradients. However, as no internal extinction correction was applied to NGC 4452, its colour gradient may naturally arise from the non-negligible presence of dust which affects the colour distribution especially along the galaxy plane, though we see no sign of dust in this galaxy. Also, we can clearly see that the red inner disc has a prominent flaring and warping. The two more reddish regions, located symmetrically with respect to the galaxy centre in the plane (depicted by two *yellow* ovals) probably point to a lens (a shelf-like feature in the surface brightness distribution) or, less likely, a ring structure. As shown in many studies, inner rings are not common in SB0 galaxies, whereas bars, often embedded in lenses of the same major-axis size, are often observed in such galaxies (Sandage 1961; Kormendy 1979, 1982; Buta, Corwin & Odewahn 2007; Kormendy 2013). Comerón et al. (2014) suggest, however, that about half of S0 galaxies have inner

rings, though many of them do not have current or recent star formation (Comerón 2013). Also, lenses are seen in some galaxies that have no bars at all (e. g., NGC 1553: Freeman 1975; Kormendy 1984, 2013). Overall, as there is no detection of H I for this galaxy in HyperLeda (Serra et al. 2012 give $\log M(\text{H I}) < 7.27$, where masses are in Solar units), the star formation is probably very low and should be consistent with what we observe in regular S0 galaxies.

As emphasized in Kormendy (1979) and based on the standard definitions and common illustrations in de Vaucouleurs (1959), Sandage (1961), Kormendy (1982, 2013), Sandage & Bedke (1994), Buta et al. (2007), bars and lenses in early-type galaxies (1) both have very slowly decreasing surface brightnesses along their long axes (along any axis, for a lens) and then a sharp outer edge (they represent 'shelves' in their surface brightness profiles); (2) bars have higher surface brightnesses than the lenses in which they are commonly embedded; (3) most often, the bar exactly fills the lens along its longest dimension. Using these facts, Kormendy & Bender (2012) clearly distinguish five Sérsic components in NGC 4452: a nuclear stellar cluster ($n = 0.7$), a small pseudo-bulge ($n = 1.1$), a bar at a skew angle (not along the line of sight and not perpendicular to it) with $n = 0.18$, a lens component (with $n = 0.2$), and an outer disc. In our decomposition we adopt the geometrical model by Kormendy & Bender (2012) for the four inner (thin or tiny in our SDSS image) components (the nucleus, the pseudo-bulge, the bar, and the lens), implying that their geometry was well fitted by Kormendy & Bender (2012) (due to the high resolution of the *HST* image used as compared to our SDSS image) and very sharp edges of the bar and the lens. Also, we assume that the geometry of these components does not change significantly for the *HST* ACS F475W and SDSS *r* filters. In our fitting, we only fit the effective surface brightnesses and C_0 of these components. Note that we adopt the ellipticities of these components from Kormendy & Bender (2012) (see their fig. 8) and keep them fixed in our decomposition. In contrast to the 1D fitting in Kormendy & Bender (2012), here we fit the overall 2D surface brightness distribution in NGC 4452 – this allows us to take into account the flattening, position angle, and discyness/boxyness parameters for the remaining components – an inner disc (which is especially visible in the colour map, see Fig. 5, as a red colour component in the main galaxy plane) and a slightly bluer tilted outer disc. In the cases of the nucleus and the bulge, which are too tiny in our SDSS image to be well resolved, the C_0 parameter is set to 0, that is it implies pure elliptical isophotes.

In total, our model consists of six components, four of which have the fixed geometry as derived in Kormendy & Bender (2012) and for the two outer components (discs) all parameters left free during the fitting. The results of our decomposition (see Table 2
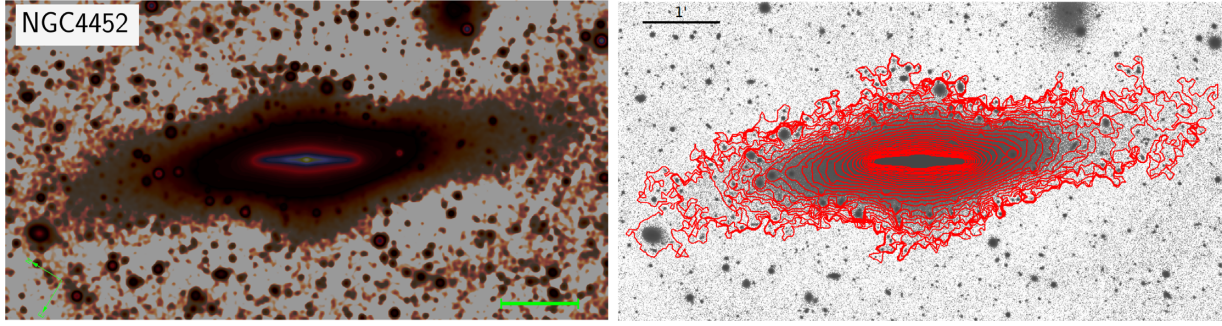
Figure 3. Stacked Legacy *grz* image for NGC 4452 (left plot) and its superimposed isophotes from 20 to 26 mag arcsec^{-2} (right plot).
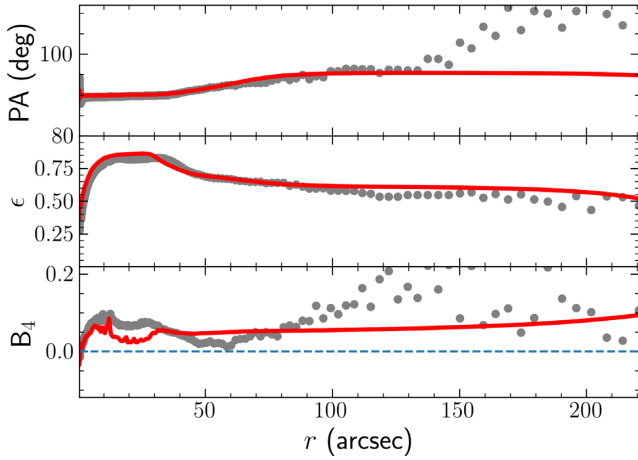

Figure 4. Results of the IRAF/ELLIPSE fitting of NGC 4452 for the stacked Legacy data. The galaxy image is rotated so that the plane of the inner structure is horizontal (the PA offset is 58.9°). The red line shows the model.
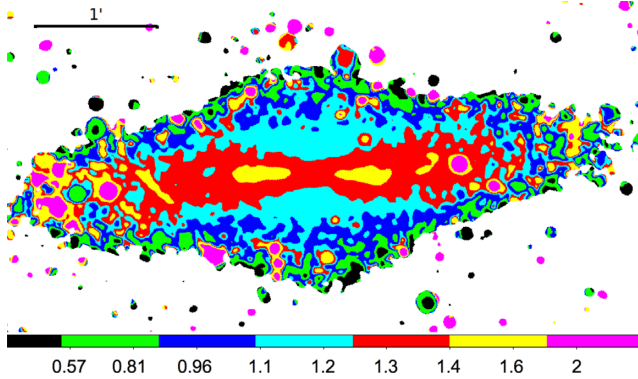

Figure 5. Colour $(g - z)$ map based on the Legacy data for NGC 4452 up to the isophote 26 mag arcsec^{-2} in the g band.

and Fig. 6) confirm that the two outer components are indeed discs – their Sérsic indices are close to 1. The radial distribution in an edge-on transparent exponential disc is described by the function r/h $K_1(r/h)$, where h is the disc scalelength and K_1 is the modified Bessel function of the second kind (van der Kruit & Searle 1981). If one fits a Sérsic function to this distribution, the Sérsic index will be $n \approx$ 0.8–0.9 – this is what we derive for both the discs in NGC 4452. Also, their negative parameters C_0 show that these components have discy, diamond-like isophotes. Interestingly, the less extended disc coincides with the plane of the inner components, whereas the outer

Table 2. Results of the IMFIT fitting NGC 4452 for the stacked SDSS image. In parentheses we list the IMFIT functions which we use for describing each galaxy component. The fixed parameters are marked by *.

| Component	Parameter	Value	Units
1. Nucleus:	PA*	90.0	deg
(*Sérsic*)	ϵ^*	0.25	
	n^*	0.68	
	$\mu_{e,r}$	16.53 ± 0.56	mag arcsec^{-2}
	r_e^*	0.11	arcsec
	r_e^*	0.009	kpc
	f	0.001 ± 0.0003	
2. Bulge:	PA*	90.0	deg
(*Sérsic*)	ϵ^*	0.7	
	n^*	1.06	
	$\mu_{e,r}$	19.00 ± 0.40	mag arcsec^{-2}
	r_e^*	2.10	arcsec
	r_e^*	0.17	kpc
	f	0.019 ± 0.008	
3. Bar:	PA*	90.0	deg
(*Sérsic_GenEllipse*)	ϵ^*	0.95	
	C_0	0.42 ± 0.33	
	n^*	0.18	
	$\mu_{e,r}$	19.12 ± 0.04	mag arcsec^{-2}
	r_e^*	11.98	arcsec
	r_e^*	0.97	kpc
	f	0.055 ± 0.001	
4. Lens:	PA*	90.0	deg
(*Sérsic_GenEllipse*)	ϵ^*	0.92	
	C_0	4.93 ± 2.35	
	n^*	0.20	
	$\mu_{e,r}$	19.75 ± 0.04	mag arcsec^{-2}
	r_e^*	23.46	arcsec
	r_e^*	1.90	kpc
	f	0.223 ± 0.004	
5. Disc:	PA	90.5 ± 0.2	deg
(*Sérsic_GenEllipse*)	ϵ	0.76 ± 0.03	
	C_0	-0.56 ± 0.35	
	n	0.80 ± 0.27	
	$\mu_{e,r}$	20.62 ± 0.30	mag arcsec^{-2}
	r_e	26.42 ± 1.48	arcsec
	r_e	2.14 ± 0.12	kpc
	f	0.398 ± 0.159	
6. Disc:	PA	95.5 ± 2.3	deg
(*Sérsic_GenEllipse*)	ϵ	0.66 ± 0.01	
	C_0	-0.72 ± 0.11	
	n	0.94 ± 0.33	
	$\mu_{e,r}$	23.29 ± 0.50	mag arcsec^{-2}
	r_e	65.93 ± 10.62	arcsec
	r_e	5.34 ± 0.86	kpc
	M_r	-18.23 ± 0.37	mag
	f	0.304 ± 0.104	
	r_{28}	3.83 ± 0.19	arcmin
	r_{28}	18.62 ± 0.93	kpc
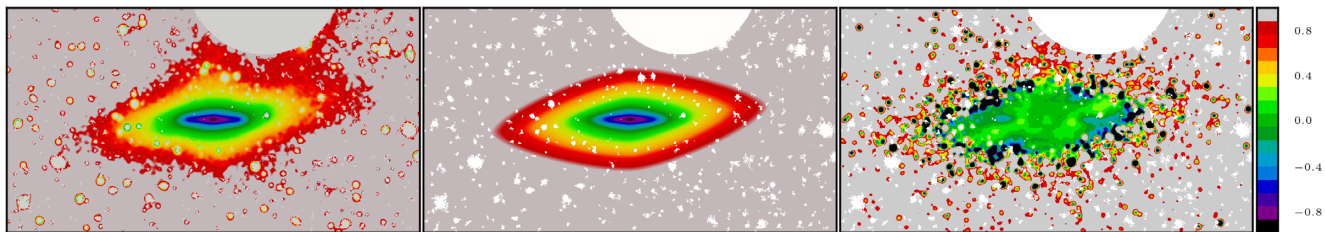
Figure 6. Results of the photometric decomposition of NGC 4452 for the stacked SDSS image: the observation (left), the model (middle), and the residual image (right), which indicates the relative deviation between the fit and the image.

disc is inclined by ∼8° with the plane of the inner structure. The outer tilted disc has a rather large contribution to the total galaxy luminosity (≈30 per cent), despite the very low deprojected central surface brightness $\mu_{0,r}^{\text{face-on}} = 22.77$ mag arcsec^{-2} (for comparison, in the EGIS catalogue $\langle\mu_{0,r}^{\text{face-on}}\rangle = 21.56 \pm 0.81$ mag arcsec^{-2}). However, its radial scalelength is also unusual ($h = 3.51$ kpc) given its very low central surface brightness (see the correlation between the face-on central surface brightness and disc scalelength in fig. 2 in Fathi 2010 and discussion in van der Kruit & Freeman 2011). It should also be noted that this disc has a very small flattening $\epsilon = 0.66$ as compared to $\langle\epsilon\rangle = 0.79 \pm 0.05$ for the EGIS galaxy discs. The inner disc, however, has typical characteristics for edge-on discs: $\langle\mu_{0,r}^{\text{face-on}}\rangle = 20.78$ mag arcsec^{-2}, $h = 1.75$ kpc, and $\epsilon = 0.76$.

In Fig. 4, we superimpose the results of the IRAF/ELLIPSE fitting for our model. One can see that the model follows the observation fairly well. The increase of the position angle at large radii points to a warp of the outer tilted disc. Taking into account the above said, the outer disc can be considered as a tilted warped thick disc, whereas the inner disc is a warped and flared thin disc.

3.3.2 NGC 4469

According to HyperLeda, this galaxy is classified as SB0-a. As NGC 4452, it also belongs to the Virgo cluster, but it is located far out from its centre (given the distance to the cluster 16.5 Mpc, the projected distance from its centre to NGC 4469 is 1.05 Mpc versus 0.24 Mpc for NGC 4452). Ciambur & Graham (2016) studied a prominent 'hump' X-structure, which represents a manifestation of a side-on bar in edge-on galaxies (see e.g. Combes et al. 1990; Lütticke, Dettmar & Pohlen 2000). According to the results of their isophote fitting, it is obvious that they do not consider the outer structure of this galaxy (see their Fig. A1): their isophotes do not extend deeper than ≈24 mag arcsec^{-2}.

Cortés, Kenney & Hardy (2015) give a detail description of NGC 4469 in their appendix and note slightly twisted outer isophotes with respect to its inner disc. However, we found that the name NGC 4469 should be replaced there by NGC 4569, as NGC 4469 does not appear anywhere else in their study, whereas NGC 4569 is truly considered.

Jo et al. (2018) detected an appreciable extraplanar Hα and UV emission, which is associated with diffuse extraplanar ionized gas and extraplanar dust. This vertically extended dust can effectively scatter UV starlight and Hα from H II regions located in the galactic plane.

Hendy et al. (2016) measure a rather strong warp of the disc in NGC 4469 by estimating the warp degree using the areas of an outer isophote and its fitted ellipse.

Mosenkov et al. (2020) detect boxy/oval ($C_0 = 0.4$) isophotes for the outer structure in NGC 4469. The HERON observation (Rich et al. 2019) of this galaxy clearly shows that the outer structure is tilted by several degrees with respect to the inner one. Here, using the SDSS and Legacy imaging, we confirm their result. Fig. 7 shows a thick boxy outer structure (a disc) which indeed has a prominent tilt. None of the deep observations, which we considered for this galaxy, does reveal any LSB details near NGC 4469.

Its inclination i, based on a patchy dust structure in the galaxy centre, was estimated in Mosenkov et al. (2020) as 88°. However, here we re-estimated the inclination based on the *GALEX* NUV image, which, together with the optical images under study, shows a ring-like structure (it is also evident from a colour map, see below). For this ring, we identified its abrupt edges and, based on its shape, we can use the formula (A1) $i = \arccos(\Delta z/R)$ from Mosenkov et al. (2015), where R is the radius of the observed ring-like structure and Δz is the maximum projected height of the inclined structure above (or below) the galaxy plane. We measured these parameters to be $R = 100.8$ arcsec and $\Delta z = 14.4$ arcsec and computed the galaxy inclination as approximately 82°.

The visual inspection of the results of the isophote fitting in Fig. 8 reveals a change of the position angle of ≈8°, starting from the radius 75 arcsec up to the outermost isophotes. The inner region within 10 arcsec shows a round ($\epsilon \approx 0$, $B_4 \approx 0$) component (bulge) which is surrounded by a prominent boxy (X-shape) bar ($B_4 < 0$ up to $r \approx 70$ arcsec). At radii 75–150 arcsec, we can see discy isophotes, which are probably related to a highly inclined inner ring. The slightly tilted outer structure at $r \gtrsim 200$ arcsec exhibits conspicuous boxy isophotes ($B_4 < 0$).

Our $(g - z)$ map in Fig. 9 obviously exhibits some traces of the patchy dust over the galaxy body (depicted by *pink* and *yellow* smudges), mainly in the central galaxy region. We can clearly see blue tips of an inner structure (possibly, a ring) and a reddish X-structure, surrounded by a blueish outer disc. The colour profile in Fig. B1 shows a very red central region (the internal extinction is one of the main reasons of this peak) and a steady blueing with radius where the disc dominates. The comparison with NGC 4452 shows that the disc of NGC 4469 is slightly redder. Nevertheless, as H I mass is estimated to be 4.9×10^7 M$_\odot$ (calculated as $M_{\text{H I}} = 2.36 \times 10^5 \times D^2 \times F_{\text{H I}}$, where the total flux $F_{\text{H I}}$ in Jy km s^{-1} is taken from table 1 in Taylor et al. 2012) and the emission lines in its SDSS spectrum are excited by star formation.

Our decomposition model for this galaxy includes four primary components: bulge, bar, ring, and disc. For uniformity, each of them is described by a Sérsic function. The results of the decomposition are listed in Table 3. The goodness of the model is shown in Fig. 10. In Fig. C1, we show a surface brightness profile with a superimposed decomposition model.

According to our decomposition results, the bulge has an exponential profile ($n \approx 1.3$) which makes it a pseudo-bulge (we admit, however, that due to internal dust extinction, the parameters
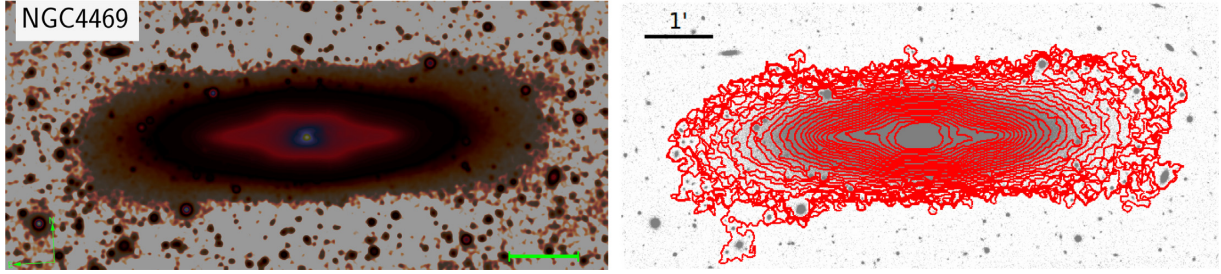
Figure 7. Stacked Legacy *grz* image for NGC 4469 (left plot) and its superimposed isophotes from 20 to 26 mag arcsec^{-2} (right plot).
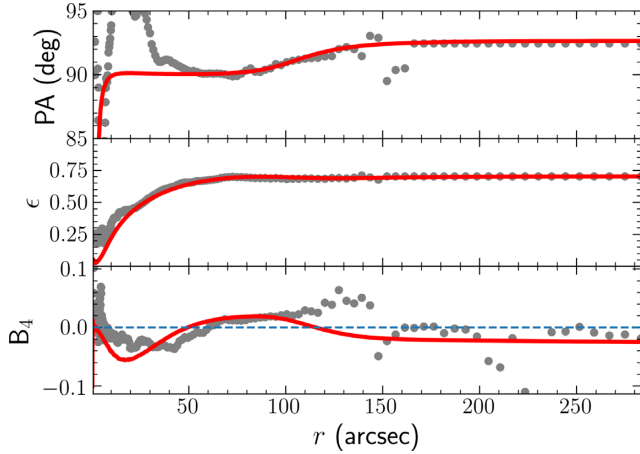

Figure 8. Results of the IRAF/ELLIPSE fitting for NGC 4469 for the stacked Legacy image. The galaxy image is rotated so that the plane of the inner structure is horizontal (the PA offset is 3.8°). The red line shows the model.
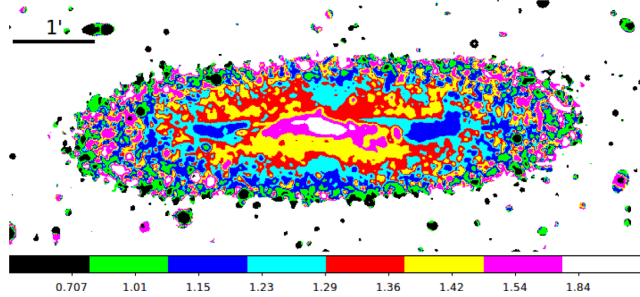

Figure 9. Colour (*g* − *z*) map based on the Legacy data for NGC 4469 up to the isophote 26 mag arcsec^{-2} in the *g* band.

Table 3. Results of the IMFIT fitting NGC 4469 for the stacked SDSS image. In parentheses we list the IMFIT functions that we use for describing each galaxy component. The fixed parameters are marked by *.

Component	Parameter	Value	Units
1. Bulge:	PA*	90	deg
(*Sérsic*)	ϵ*	0.0	
	n	1.27 ± 0.06	
	$\mu_{e,r}$	20.0 ± 0.13	mag arcsec^{-2}
	r_e	4.69 ± 0.49	arcsec
	r_e	0.38 ± 0.04	kpc
	f	0.055 ± 0.007	
2. Bar:	PA	89.9 ± 1.1	deg
(*Sérsic_GenEllipse*)	ϵ	0.27 ± 0.01	
	C_0	9.2 ± 3.1	
	n	0.77 ± 0.22	
	$\mu_{e,r}$	21.17 ± 0.11	mag arcsec^{-2}
	r_e	19.14 ± 5.43	arcsec
	r_e	1.55 ± 0.44	kpc
	f	0.221 ± 0.053	
3. Ring:	PA	90.0 ± 0.5	deg
(*Sérsic_GenEllipse*)	ϵ	0.79 ± 0.01	
	C_0	-0.4 ± 0.1	
	n	0.38 ± 0.07	
	$\mu_{e,r}$	21.27 ± 0.05	mag arcsec^{-2}
	r_e	62.35 ± 7.78	arcsec
	r_e	5.05 ± 0.63	kpc
	f	0.387 ± 0.086	
4. Disc:	PA	93.1 ± 0.4	deg
(*Sérsic_GenEllipse*)	ϵ	0.69 ± 0.02	
	C_0	0.5 ± 0.2	
	n	0.81 ± 0.22	
	$\mu_{e,r}$	23.25 ± 0.19	mag arcsec^{-2}
	r_e	90.25 ± 2.47	arcsec
	r_e	7.31 ± 0.20	kpc
	M_r	-19.07 ± 0.19	mag
	f	0.337 ± 0.035	
	r_{28}	5.10 ± 0.34	arcmin
	r_{28}	24.78 ± 1.67	kpc

of the bulge may be unreliable). The bright bar is significantly puffed up in the vertical direction ($\epsilon = 0.3$). Its profile is close to exponential ($n \approx 0.8$) and the isophotes are extremely boxy ($C_0 = 9$), which can be explained by the tremendous X-structure. Many or even most well developed bars have gone through a phase of vertical buckling instability that results in a boxy-shaped or even X-shaped inner structure (Combes & Sanders 1981; Combes et al. 1990; Pfenniger & Norman 1990; Pfenniger & Friedli 1991; Raha et al. 1991; Athanassoula & Misiriotis 2002; Athanassoula 2005; Martinez-Valpuesta, Shlosman & Heller 2006; Smirnov & Sotnikova 2019). The third component, which looks like a diamond-like disc, has a small Sérsic index ($n \approx 0.4$) and shows a smooth truncation at $\mu_r = 21.8$ mag arcsec^{-2}. We suppose that this component more closely resembles a ring (or, less likely, a tightly wound spiral). Its blue colour, unlike the reddish bar, shows that this component

probably is not a lens (Herrera-Endoqui et al. 2017). The outer disc, as in the case of NGC 4452, is also close to exponential ($n \approx 0.8$), but, in contrast, has boxy isophotes ($C_0 = 0.5$). Similar to NGC 4452, its luminosity fraction f is about 34 per cent. The disc has a very low surface brightness ($\mu_{0,r}^{\text{face}-\text{on}} = 23.11$ mag arcsec^{-2}), while the radial extent is quite large for its luminosity (its scalelength $h = 5.95$ kpc is larger than that of our Milky Way, see van der Kruit & Freeman 2011 and references therein). According to our decomposition results, the difference between the position angles for the inner and outer structures is 3.5°.
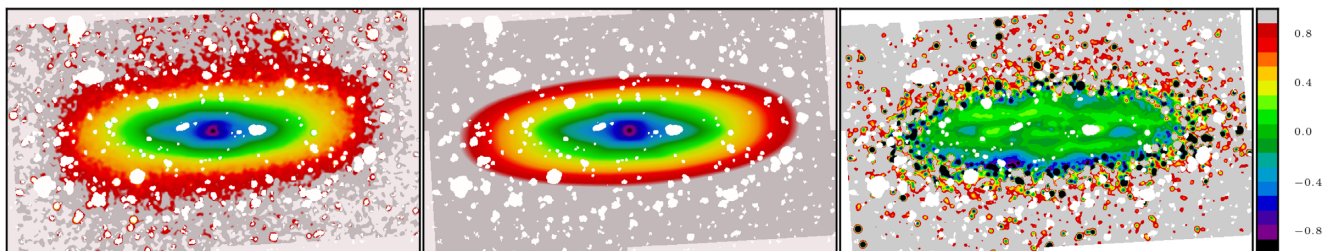
Figure 10. Results of the photometric decomposition of NGC 4469 for the stacked SDSS image: the observation (left), the model (middle), and the residual image (right), which indicates the relative deviation between the fit and the image.
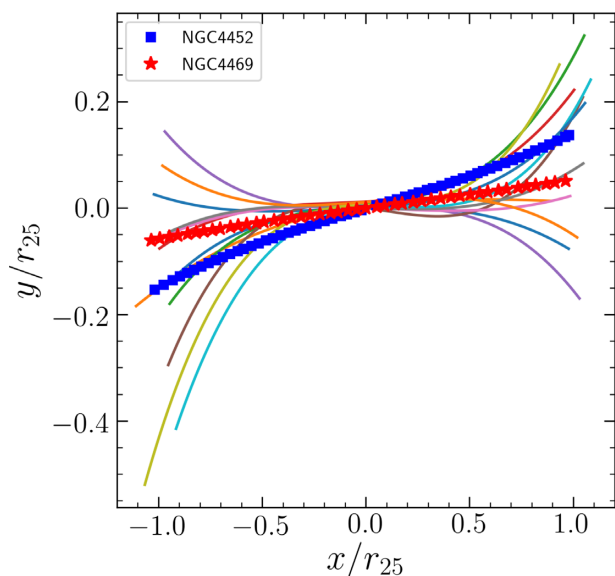

Figure 11. Centrelines for the galaxies with conspicuous warps from Reshetnikov et al. (2016) compared to the two galaxies with tilted outer structures, which we consider in this paper. All centrelines were plotted for isophotes of 25.5 mag arcsec^{-2} in the *r* band and approximated by splines. The *x* and *y* dimensions for each galaxy are normalized by its optical radius r_{25}.

In Fig. 8, we superimpose the results of the IRAF/ELLIPSE fitting for the model. As one can see, except for the central region, where the galaxy light is significantly affected by the dust attenuation (although the dusty patches were masked out during the fitting), the model follows the observation fairly well.

4 DISCUSSION

In this section, we discuss possible reasons of the observed phenomenon of the tilted discs in NGC 4452 and NGC 4469.

4.1 Tilted disc or warps?

To show that the tilted outer structures in NGC 4452 and NGC 4469 do not resemble ordinary warps of galactic discs, we collected the centrelines of 13 galaxies with conspicuous optical warps from Reshetnikov et al. (2016). These centrelines were created for isophotes of 25.5 mag arcsec^{-2} in the *r* band. For the galaxies, which we study in this paper, we also created centrelines for the same isophote (see Fig. D1). Prior to that, their stacked images were interpolated in the masked regions. As one can see in Fig. 11, the centrelines of the outermost isophotes for the galaxies with tilted

outer structures are virtually straight lines (their position angles are constant with radius), except that NGC 4452 shows some warping far from the galaxy centre, whereas the centrelines for the galaxies with warps are appreciably curved. In Fig. D1, we pay your attention that the minor axes of the outermost isophotes for both galaxies are not perpendicular to their general galaxy planes (major axes of the inner isophotes).

A more straightforward way to compare the warps from Reshetnikov et al. (2016) and the 'warps' in NGC 4452 and NGC 4469 is to compare the parameters of their warps, the warp angle Ψ (an angle measured between the galaxy plane and the line connecting the galaxy centre and the tips of the outer 25.5 isophote) and the radius r_w where the warp begins (see Fig. 1). We created centrelines for each of the isophotes plotted and then averaged them. That resulted in a final centreline which was then fitted with a double piecewise linear function (see Reshetnikov et al. 2016 for details). In Fig. D1 by red lines we show the centrelines for each of the galaxies. For NGC 4452, we obtained $r_w = (0.18 \pm 0.02) r_{25}$, $\Psi_{NW} = -7.6°$ (north-west, or left warp), and $\Psi_{SE} = 10.2°$ (south-east, or right warp). For NGC 4469, $r_w = (0.60 \pm 0.03) r_{25}$, $\Psi_S = -5.5°$ (south, or left warp), and $\Psi_N = 5.6°$ (north, or right warp). For comparison, in Reshetnikov et al. (2016), $\langle\Psi\rangle = 7.3 \pm 6.4°$, and $\langle r_w \rangle = (0.90 \pm 0.24) r_{25}$. We can see that the warps in both galaxies start at smaller radii (especially in NGC 4452) than observed in galaxies with prominent warps. Also, our models of NGC 4452 and NGC 4469, which do not imply warping of the outer discs but only their different position angles with respect to the inner components, describe the observations fairly well, including the major axis profiles, as well as PA, ellipticity, and B_4 distributions. From this we can conclude that if the observed outer structures in NGC 4452 and NGC 4469 truly are genuine disc warps, they do not appear typical and deserve a special attention in any event.

4.2 Triaxiality of the outer or inner structure?

Another important issue regarding the tilted structures is the projection effect, when the galaxy inclination and a specific orientation of a triaxial component in this galaxy can give us an illusion that the inner or outer structure is tilted with respect to the outer or inner galaxy region, respectively.

As NGC 4469 is not a pure edge-on galaxy and has a bright triaxial bar, the projection effect cannot be neglected. To show this, we performed numerical simulations to create mock galaxies with B/PS bulges (see details in the Appendix E). By changing the galaxy inclination angle and position angle of the bar (the angle between the line of nodes and the line of sight from the galaxy centre to the observer), we can indeed find a combination of these two angles, which gives us an appearance of a galaxy with a tilted inner structure (see Fig. 12, top left hand panel). Interestingly, in the EGIS catalogue
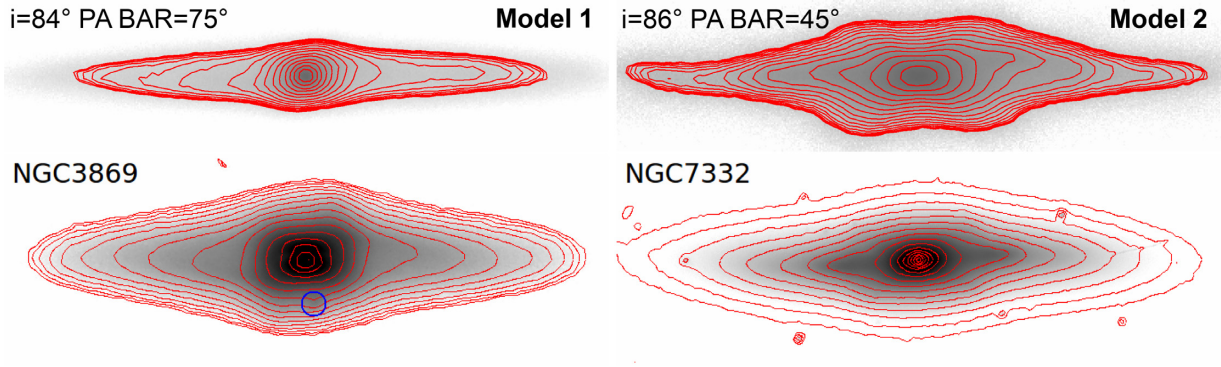
Figure 12. *Top panels:* Two different simulations of galaxies with the specific inclinations and position angles of the bar/bar plus the lens, which illustrate the effect of the 'inner tilting'. *Bottom panels:* Real galaxies that demonstrate the same effect. The blue circle shows a satellite.

we found a galaxy, NGC 3869 (see Fig. 12, bottom left hand panel), which resembles the mock galaxy (Model 1) – its inner structure looks tilted and, moreover, its X-shape structure seems asymmetric (note that in the image under the boxy B/PS bulge, there is also a satellite shown by the blue circle). The distributions of position angle, ellipticity, and B_4 with radius for NGC 3869 and the mock galaxy are presented in Fig. E1. Both galaxies show very similar distributions of these quantities. Therefore, it is highly likely that the asymmetric view and the tilt of the inner structure (bar) in NGC 3869 is, in fact, a consequence of a projection effect. A similar effect is observed in NGC 7332, where we can see a B/PS bulge with relatively bright ansae (Fig. 12, bottom right hand panel). In another simulation of ours, Model 2, (Fig. 12, top right hand panel), a bar with a lens and bright ansae naturally arise in the course of the model evolution. By changing the galaxy inclination and position angle of the bar, we can again obtain a projection where the inner structure is inclined with respect to the disc. NGC 7332 was noted by Michard & Marchal (1993) among other 10 galaxies with tilted inner structures. Most of these galaxies also harbour bars, therefore the observed tilting in these galaxies can probably be explained by the same effect of projection, as in the case of NGC 3869 and NGC 7332. For a pedagogical purpose, in Appendix A we discuss another galaxy, NGC 509 from the HERON sample. This galaxy was initially selected for this paper as a galaxy with a tilted outer structure, but after a careful investigation we rejected it because its orientation is far from edge-on.

As to NGC 4469, apart from the B/PS bulge it has an inner ring-like structure. As this structure should, in principle, be almost round (inner rings typically have axial ratios of 0.8–0.85, see e.g. Buta 1995; Kormendy 2013; Comerón et al. 2014), the orientation of its major axis should not strongly depend on the galaxy inclination and the position angle of the bar.

We note, however, that not only bars, bulges, and lenses can be triaxial structures (Kormendy 1979; Méndez-Abreu et al. 2010; Sotnikova, Reshetnikov & Mosenkov 2012; Costantin et al. 2018), but also large-scale discs. For example, in the lenticular galaxy NGC 5485 Sil'chenko (2016) found a non-circular stellar exponential disc with a highly non-circular stellar rotation. Also, she detected two wide elliptical stellar rings in the unbarred lenticular galaxy NGC 502, which might be formed due to a dry minor merging. Galaxies with such oval distortions or elliptical discs may be not so rare.

The triaxiality of the stellar haloes is still under question. For example, haloes in hybrid semi-analytic plus *N*-body models by Bullock & Johnston (2005) are oblate (see also Bell et al. 2008),

whereas Cooper et al. (2010) find triaxial haloes in their *N*-body only simulations of Milky Way-mass galaxies (see also Bailin et al. 2014). In recent large volume cosmological hydrodynamical simulation Illustris (Vogelsberger et al. 2014), Elias et al. (2018) found triaxial stellar haloes in galaxies with a wide range of the stellar halo fraction: $0.6 \lesssim b/a \lesssim 1.0$ and $0.4 \lesssim c/a \lesssim 0.9$ (in their notation, *a*, *b*, *c* are the major to minor principal axes of the inertia tensor for the stars). However, they concluded that the simulated haloes can be fairly oblate, with median $\langle b/a \rangle \sim 0.9$ and $\langle c/a \rangle \sim 0.5$. Monachesi et al. (2019) came to the same conclusion: they studied halo global properties in the Auriga cosmological magnetohydrodynamical high-resolution simulations of Milky Way-mass galaxies (Grand et al. 2017): most of the Auriga haloes appeared to be oblate spheroids as well.

For the Milky Way, it has been well-established that the shape of the stellar halo is an oblate, not a triaxial spheroid (Yanny et al. 2000; Larsen & Humphreys 2003; Jurić et al. 2008; Deason, Belokurov & Evans 2011). Observationally, it is shown that the stellar haloes are moderately flattened spheroids ($c/a \sim 0.6$ with a considerable range) with surface brightness distributions that are well described by a $r^{-\alpha}$ law, where the power slope α is usually found to be 2–4 (see e.g. Zibetti & Ferguson 2004; Harmsen et al. 2017), supported by cosmological hydrodynamical simulations by Font et al. (2011).

In conclusion, if we assume that the outer component in NGC 4469 has a triaxial shape (although the observations show that the outer structures in disc galaxies are more likely to be oblate spheroids), whether it is a thick disc or a bright flattened exponential halo, its triaxiality may be responsible for the observed difference in the position angles of the inner and outer structures.

4.3 Misalignment between angular momenta of the disc and dark matter halo

Now, let us turn to some possible explanations of the observed phenomenon of the tilted outer structures if we suppose that they are real and not due to a projection effect.

There is every reason to expect (see e.g. Dekel & Shlosman 1983; Ostriker & Binney 1989; Katz & Gunn 1991; Binney 1992; Dubinski & Kuijken 1995; Shen & Sellwood 2006; van der Kruit & Freeman 2011) that the baryons that end up in the inner parts of a galaxy disc get accreted with an angular momentum vector (1) that is different from that of the dark matter that is accreted from the cosmic web and that lands farther out, (2) that is different from that of

baryonic gas that cools from the warm-hot intergalactic medium (see also Davé et al. 2001) and that lands in an outer disc, and (3) that is different from that of any satellites made of dark matter and baryons that may be accreted at large radii into the outer disc and/or the dark halo. Cosmological, hydrodynamic simulations show that angular momentum vectors of the gas and dark matter in haloes tend to be misaligned (van den Bosch et al. 2002; Chen, Jing & Yoshikaw 2003; Sharma & Steinmetz 2005; Sharma, Steinmetz & Bland-Hawthorn 2012). All these processes can induce tilting of the outer structure with respect to the inner one. Therefore, misalignments of main discs with outer discs whose inclinations reflect the gravity of misaligned outer dark matter haloes are certainly to be expected. However, as observationally we find few galaxies with tilted outer structures, these mechanisms should not be very important for inducing the tilts which can be directly observed (see also below).

4.4 Dark matter halo tumbling

As shown in a number of early (Binney 1978; Barnes & Efstathiou 1987; Frenk et al. 1988; Warren et al. 1992; Jing et al. 1995; Thomas et al. 1998; Yoshida et al. 2000) and more recent works (Bryan et al. 2013; Zhu et al. 2016), dark matter haloes are generally triaxial (see the review by Zasov et al. 2017). The flattened potential of triaxial haloes can induce oval distortions and non-circular velocities (Hayashi, Navarro & Springel 2007) which can be quite strong in dwarf (Valenzuela et al. 2007) and low-surface brightness galaxies (Hayashi & Navarro 2006). Its triaxiality can rapidly change over time Vera-Ciro et al. (2011) – this can impart a significant external torque on the galaxy disc. Dubinski & Chakrabarty (2009) performed *N*-body simulations and considered the inner part of the dark matter to be aligned with the disc, while the outer dark matter halo is misaligned and slowly tumbling. They found that the misaligned and tumbling outer halo causes a slowly changing external torque on the disc and that, in its turn, induces long-lived transient warps and tilting (see also Toomre 1983; Sparke & Casertano 1988; Ostriker & Binney 1989; Kuijken 1991; Debattista & Sellwood 1999; Jiang & Binney 1999), bar instabilities (Dubinski & Chakrabarty 2009) and spiral structure (see also Khoperskov et al. 2013; Khoperskov & Bertin 2015; Hu & Sijacki 2016). Therefore, this effect can be at play to explain the observed tilting in the galaxies under study. Unfortunately, this mechanism cannot be verified observationally. Also, the recent study by Earp et al. (2019) showed that the dark matter halo by itself does not play a significant role in the disc tilting.

4.5 Accretion

S0 galaxies are often thought to be red and dead systems without current star formation. However, this claim has been challenged and evaluated in multiple studies of S0 galaxies (see e.g. recent studies by Kostiuk & Sil'chenko 2015; Sil'chenko et al. 2018; Proshina, Kniazev & Sil'chenko 2019; Sil'chenko et al. 2019; Proshina et al. 2020). In recent study, for example, Proshina et al. (2020) considered the ring S0 galaxy NGC 4513. They found that its ionized gas counterrotates the stellar component and, therefore, it was accreted. They concluded that its blue ring, demonstrating current star formation, is a result of tidal disruption of a massive gas-rich neighbour in the past, or it may be a consequence of a long star-formation event provoked by a gas accretion from a cosmological filament. Strongly inclined ionized gas discs, observed in many S0 galaxies (Katkov et al. 2015; Sil'chenko et al. 2019), is another evidence of the external gas supply. As Sil'chenko et al. (2019) claim,

'a crucial difference of the accretion regime in S0s with respect to spirals: the geometry of gas accretion in S0s is typically off-plane'.

Recent accretion of a gas-rich satellite in the case of NGC 4452 seems to be impossible by two reasons. First, most galaxies in the central region of the Virgo cluster are gas-poor galaxies due to, for example, ram pressure stripping. Secondly, the velocity dispersion of galaxies in a cluster is very high (approximately, up to several thousands of km s^{-1}). Therefore, a fast encounter does not result in merging, but in galaxy harassment (see Section 4.6).

In the case of NGC 4469, which is located quite far from the Virgo centre, an accretion of one or a few gas-rich dwarfs might happened several Gyr ago. One of such events can be responsible for a fairly blue ring in this galaxy.

Another possible scenario to form tilted structures might be gas accretion via cosmological filaments when thin filaments come into a galaxy under some angle and make an inclined gaseous disc (Thakar & Ryden 1996, 1998; Kereš et al. 2005; Dekel & Birnboim 2006) with ongoing star formation. However, in the presence of X-ray emitting, hot gas in the Virgo cluster (especially in its central part where NGC 4452 resides), it is hard to explain how gas accretion via filaments can act in such harsh conditions.

4.6 Tidally induced tilts and warps

We suppose that the most plausible explanation of the observed tilted discs in NGC 4452 and NGC 4469 is galaxy harassment when high-speed encounters of galaxies in a cluster do not result in a merger but significantly affect the shape (and morphology) of the interacting galaxies which cause the discs to warp and tilt. Numerical and cosmological simulations support this mechanism (Vesperini & Weinberg 2000; Kim et al. 2014; Semczuk et al. 2020).

As Kormendy & Bender (2012) noted, similar to NGC 4762, the outer disc in NGC 4452 is thick, warped, and tidally distorted. This could have been caused by a gravitational encounter with IC 3381. Note that twists of outer isophotes, observed in some galaxies, can be the result of tidal effects (see e.g. the case of NGC 205 in the vicinity of M 31, Kormendy 1982). Therefore, if we had observed the same galaxies from the edge, their outer structure would have appeared tilted with respect to the inner one.

The tilt of the outer structure in NGC 4469 can have the same reason. Galaxy harassment has plausibly heated the outer disc of NGC 4469 (meanwhile the bar has almost inevitably heated the inner disc), with time now for all the heating to have phase-mixed around the galaxy, leaving the disc thicker and very likely tilted with respect to the inner disc.

Circumstantial evidence of this mechanism in NGC 4452 and NGC 4469 can be the presence of disc antitruncations in both galaxies (see Fig. C1). As shown in multiple studies (see e.g. Erwin, Beckman & Pohlen 2005; Erwin, Pohlen & Beckman 2008), disc antitruncations can be produced by galaxy interactions.

Why is the effect of the tilting so rare (only three galaxies, including NGC 4638, have been noticed so far)? This is one of few studies (see also Michard & Marchal 1993; Mosenkov et al. 2020) where we observationally confirm this phenomenon, whereas the disc flaring, warping, and lopsidedness are often seen in edge-on galaxies and have been extensively studied for decades (Sancisi 1976; Reshetnikov & Combes 1998; Jog & Combes 2009; Comerón et al. 2011; López-Corredoira & Molgó 2014; Reshetnikov et al. 2016). The main reason of the lack of observational evidence of tilted discs and haloes is that these outer structures are not well seen in regular images, whereas in deep observations we can better visualize faint structures, including tilted envelopes. We suppose

that this phenomenon should be common in dense massive galaxy clusters. Apparently, the number of galaxies with tilted structures will increase, as more and more deep observations of galaxies become available.

5 CONCLUSIONS

In this paper, we have considered two moderate-luminosity SB0 galaxies with prominent tilted outer structures. Using different optical images (SDSS and Legacy) and by means of the stacking of the galaxy images in different bands, we were able to increase the depth of the resultant images up to 28.3 mag arcsec^{-2} for the Legacy and 27.6 for the SDSS survey. We performed isophote fitting and a complex photometric decomposition for each galaxy. Based on the obtained results, we report that these galaxies plausibly show a real tilting of the outer structure with respect to the inner region (i.e. the outer and inner structures are oriented in different, tilted planes), which cannot be only explained by disc warps (though this effect can also be present). For NGC 4452 we obtained $\Delta PA \approx 6°$, whereas for NGC 4469 the tilt is lower but still prominent ($\Delta PA \approx 3°$). The outer discs in these galaxies have completely different shapes (discy, or diamond-like, in NGC 4452 and boxy in NGC 4469).

We propose that some combination of a single high speed encounter and the cumulative effect of galaxy harassment (in different proportions), which can distort and tilt the outer galaxy structure in a cluster, is a more plausible explanation of the observed phenomenon of disc tilting in both galaxies. Another important scenario can be misalignment of the triaxial (oblate) dark matter halo and its inner stellar disc simply because of how dark matter haloes grow out of the cosmic hierarchy. In addition to that, the tumbling of the dark matter halo might be enhanced by a fast encounter several Gyr ago, which would cause the outer disc to tilt. Also, for NGC 4469, another explanation of the observed tilt, which cannot be rejected, unless a thorough kinematic study is carried out, is a possible triaxiality of an outer disc (or flat halo) in a highly inclined (but not purely edge-on) galaxy. In spite of the slightly blue colour of the tilted outer structures in both galaxies (NGC 4469 also harbours a blueish inner structure, possibly, a ring), which can be evidence of ongoing star formation from the gas captured due to accretion of several gas-rich dwarfs several Gyr ago, this mechanism seems to be far less likely to form a tilted outer structure (especially for NGC 4452) in the troublesome Virgo cluster where encounters are too fast for accretion to occur.

In our future paper, we are about to study the nature of the main structural components in NGC 4469 and NGC 4452 using deep 21 cm H I observations, optical spectral observations, and kinematic measurements.

Using numerical simulations, we also showed that tilted inner structures may be well explained by a specific galaxy inclination, together with a specific orientation of a triaxial inner component (bar, bulge, and lens) with respect to the observer.

at the Ohio State University, the Mitchell Institute for Fundamental Physics and Astronomy at Texas A&M University, Financiadora de Estudos e Projetos, Fundacao Carlos Chagas Filho de Amparo, Financiadora de Estudos e Projetos, Fundacao Carlos Chagas Filho de Amparo a Pesquisa do Estado do Rio de Janeiro, Conselho Nacional de Desenvolvimento Cientifico e Tecnologico and the Ministerio da Ciencia, Tecnologia e Inovacao, the Deutsche Forschungsgemeinschaft and the Collaborating Institutions in the Dark Energy Survey. The Collaborating Institutions are Argonne National Laboratory, the University of California at Santa Cruz, the University of Cambridge, Centro de Investigaciones Energeticas, Medioambientales y Tecnologicas-Madrid, the University of Chicago, University College London, the DES-Brazil Consortium, the University of Edinburgh, the Eidgenossische Technische Hochschule (ETH) Zurich, Fermi National Accelerator Laboratory, the University of Illinois at Urbana-Champaign, the Institut de Ciencies de l'Espai (IEEC/CSIC), the Institut de Fisica d'Altes Energies, Lawrence Berkeley National Laboratory, the Ludwig-Maximilians Universitat Munchen and the associated Excellence Cluster Universe, the University of Michigan, the National Optical Astronomy Observatory, the University of Nottingham, the Ohio State University, the University of Pennsylvania, the University of Portsmouth, SLAC National Accelerator Laboratory, Stanford University, the University of Sussex, and Texas A&M University.

BASS is a key project of the Telescope Access Program (TAP), which has been funded by the National Astronomical Observatories of China, the Chinese Academy of Sciences (the Strategic Priority Research Program 'The Emergence of Cosmological Structures' Grant # XDB09000000), and the Special Fund for Astronomy from the Ministry of Finance. The BASS is also supported by the External Cooperation Program of Chinese Academy of Sciences (Grant # 114A11KYSB20160057), and Chinese National Natural Science Foundation (Grant # 11433005).

The Legacy Survey team makes use of data products from the Near-Earth Object Wide-field Infrared Survey Explorer (NEOWISE), which is a project of the Jet Propulsion Laboratory/California Institute of Technology. NEOWISE is funded by the National Aeronautics and Space Administration.

The Legacy Surveys imaging of the DESI footprint is supported by the Director, Office of Science, Office of High Energy Physics of the U.S. Department of Energy under Contract No. DE-AC02-05CH1123, by the National Energy Research Scientific Computing Center, a DOE Office of Science User Facility under the same contract; and by the U.S. National Science Foundation, Division of Astronomical Sciences under Contract No. AST-0950945 to NOAO.

This publication makes use of data products from the Wide-field Infrared Survey Explorer, which is a joint project of the University of California, Los Angeles, and the Jet Propulsion Laboratory/California Institute of Technology, funded by the National Aeronautics and Space Administration.

This study makes use of observations made with the NASA Galaxy Evolution Explorer. *GALEX* is operated for NASA by the California Institute of Technology under NASA contract NAS5-98034.

DATA AVAILABILITY

The data underlying this article will be shared on reasonable request to the corresponding author.

REFERENCES

Ahumada R. et al., 2020, ApJS, 249, 3
Ann H. B., Bae H. J., 2016, J. Korean Astron. Soc., 49, 239
Ann H. B., Park J. C., 2006, New Astron., 11, 293
Athanassoula E., 2005, MNRAS, 358, 1477
Athanassoula E., Misiriotis A., 2002, MNRAS, 330, 35
Athanassoula E., Morin S., Wozniak H., Puy D., Pierce M. J., Lombard J., Bosma A., 1990, MNRAS, 245, 130
Bailin J., Steinmetz M., 2004, ApJ, 616, 27
Bailin J., Bell E. F., Valluri M., Stinson G. S., Debattista V. P., Couchman H. M. P., Wadsley J., 2014, ApJ, 783, 95
Barnes J., Efstathiou G., 1987, ApJ, 319, 575
Battaner E., Jimenez-Vicente J., 1998, A&A, 332, 809
Battaner E., Florido E., Sanchez-Saavedra M. L., 1990, A&A, 236, 1
Bell E. F. et al., 2008, ApJ, 680, 295
Bertin E., Arnouts S., 1996, A&AS, 117, 393
Bertola F., Buson L. M., Zeilinger W. W., 1992, ApJ, 401, L79
Bett P. E., Frenk C. S., 2012, MNRAS, 420, 3324
Bianchi L., Conti A., Shiao B., 2014, Adv. Space Res., 53, 900
Bianchi S. et al., 2018, A&A, 620, A112
Binney J., 1978, MNRAS, 183, 779
Binney J., 1992, ARA&A, 30, 51
Bizyaev D. V., Kautsch S. J., Mosenkov A. V., Reshetnikov V. P., Sotnikova N. Y., Yablokova N. V., Hillyer R. W., 2014, ApJ, 787, 24
Bosma A., 1981, AJ, 86, 1825
Boucaud A., Bocchio M., Abergel A., Orieux F., Dole H., Hadj-Youcef M. A., 2016, A&A, 596, A63
Briggs F. H., 1990, ApJ, 352, 15
Bryan S. E., Cress C. M., 2007, MNRAS, 380, 657
Bryan S. E., Kay S. T., Duffy A. R., Schaye J., Dalla Vecchia C., Booth C. M., 2013, MNRAS, 429, 3316
Bullock J. S., Johnston K. V., 2005, ApJ, 635, 931
Buta R., 1995, ApJS, 96, 39
Buta R. J., Corwin H. G., Odewahn S. C., 2007, The de Vaucouleurs Atlas of Galaxies. Cambridge Univ. Press, Cambridge
Cappellari M. et al., 2011, MNRAS, 413, 813
Chen D. N., Jing Y. P., Yoshikaw K., 2003, ApJ, 597, 35
Ciambur B. C., Graham A. W., 2016, MNRAS, 459, 1276
Ciotti L., Bertin G., 1999, A&A, 352, 447
Combes F., Sanders R. H., 1981, A&A, 96, 164
Combes F., Debbasch F., Friedli D., Pfenniger D., 1990, A&A, 233, 82
Comerón S., 2013, A&A, 555, L4
Comerón S. et al., 2011, ApJ, 741, 28
Comerón S. et al., 2014, A&A, 562, A121
Comerón S., Salo H., Knapen J. H., 2018, A&A, 610, A5
Consolandi G., Gavazzi G., Fumagalli M., Dotti M., Fossati M., 2016, A&A, 591, A38
Cooper A. P. et al., 2010, MNRAS, 406, 744
Cortés J. R., Kenney J. D. P., Hardy E., 2015, ApJS, 216, 9
Costantin L., Méndez-Abreu J., Corsini E. M., Eliche-Moral M. C., Tapia T., Morelli L., Dalla Bontà E., Pizzella A., 2018, A&A, 609, A132
Davé R. et al., 2001, ApJ, 552, 473
Davis T. A. et al., 2011, MNRAS, 417, 882
de Grijs R., van der Kruit P. C., 1996, A&AS, 117, 19
Deason A. J., Belokurov V., Evans N. W., 2011, MNRAS, 416, 2903
Debattista V. P., Sellwood J. A., 1999, ApJ, 513, L107
Debattista V. P., van den Bosch F. C., Roškar R., Quinn T., Moore B., Cole D. R., 2015, MNRAS, 452, 4094
DeBuhr J., Ma C.-P., White S. D. M., 2012, MNRAS, 426, 983
Dehnen W., 2002, J. Comput. Phys., 179, 27
Dekel A., Birnboim Y., 2006, MNRAS, 368, 2
Dekel A., Shlosman I., 1983, in Athanassoula E., ed., Proc. IAU Symp. 100, Internal Kinematics and Dynamics of Galaxies. Kluwer, Dordrecht, p. 187
Dey A. et al., 2019, AJ, 157, 168
de Vaucouleurs G., 1959 , Handbuch der Physik Vol. 53. p. 275

Dubinski J., Chakrabarty D., 2009, ApJ, 703, 2068

Dubinski J., Kuijken K., 1995, ApJ, 442, 492

Earp S. W. F., Debattista V. P., Macciò A. V., Wang L., Buck T., Khachaturyants T., 2019, MNRAS, 488, 5728

Elias L. M., Sales L. V., Creasey P., Cooper M. C., Bullock J. S., Rich R. M., Hernquist L., 2018, MNRAS, 479, 4004

Erwin P., 2015, ApJ, 799, 226

Erwin P., Beckman J. E., Pohlen M., 2005, ApJ, 626, L81

Erwin P., Pohlen M., Beckman J. E., 2008, AJ, 135, 20

Fall S. M., Efstathiou G., 1980, MNRAS, 193, 189

Fathi K., 2010, ApJ, 722, L120

Ferrarese L. et al., 2006, ApJS, 164, 334

Fliri J., Trujillo I., 2016, MNRAS, 456, 1359

Font A. S., McCarthy I. G., Crain R. A., Theuns T., Schaye J., Wiersma R. P. C., Dalla Vecchia C., 2011, MNRAS, 416, 2802

Freeman K. C., 1975, in Hayli A., ed., Proc. IAU Symp. 69, Dynamics of the Solar Systems. Kluwer, Dordrecht, p. 367

Frenk C. S., White S. D. M., Davis M., Efstathiou G., 1988, ApJ, 327, 507

Fukugita M., Ichikawa T., Gunn J. E., Doi M., Shimasaku K., Schneider D. P., 1996, AJ, 111, 1748

Gilhuly C. et al., 2019, preprint (arXiv:1910.05358)

Grand R. J. J. et al., 2017, MNRAS, 467, 179

Greggio L., Renzini A., 1990, ApJ, 364, 35

Guijarro A., Peletier R. F., Battaner E., Jiménez-Vicente J., de Grijs R., Florido E., 2010, A&A, 519, A53

Harmsen B., Monachesi A., Bell E. F., de Jong R. S., Bailin J., Radburn-Smith D. J., Holwerda B. W., 2017, MNRAS, 466, 1491

Hayashi E., Navarro J. F., 2006, MNRAS, 373, 1117

Hayashi E., Navarro J. F., Springel V., 2007, MNRAS, 377, 50

Heckman T. M., Armus L., Miley G. K., 1990, ApJS, 74, 833

Hendy Y. H. M., Samir R. M., Shaker A. A., Ibrahim A. I., 2016, NRIAG J. Astron. Geophys., 5, 269

Herrera-Endoqui M., Salo H., Laurikainen E., Knapen J. H., 2017, A&A, 599, A43

Hou L. G., Han J. L., 2014, A&A, 569, A125

Hu S., Sijacki D., 2016, MNRAS, 461, 2789

Huang S., Carlberg R. G., 1997, ApJ, 480, 503

Ideta M., Hozumi S., Tsuchiya T., Takizawa M., 2000, MNRAS, 311, 733

Infante-Sainz R., Trujillo I., Román J., 2020, MNRAS, 491, 5317

Jedrzejewski R. I., 1987, MNRAS, 226, 747

Jiang I.-G., Binney J., 1999, MNRAS, 303, L7

Jing Y. P., Mo H. J., Borner G., Fang L. Z., 1995, MNRAS, 276, 417

Jog C. J., Combes F., 2009, Phys. Rep., 471, 75

Jo Y.-S., Seon K.-i., Shinn J.-H., Yang Y., Lee D., Min K.-W., 2018, ApJ, 862, 25

Jurić M. et al., 2008, ApJ, 673, 864

Katkov I. Y., Moiseev A. V., Sil'chenko O. K., 2011, ApJ, 740, 83

Katkov I. Y., Sil'chenko O. K., Afanasiev V. L., 2013, ApJ, 769, 105

Katkov I. Y., Sil'chenko O. K., Afanasiev V. L., 2014, MNRAS, 438, 2798

Katkov I. Y., Kniazev A. Y., Sil'chenko O. K., 2015, AJ, 150, 24

Katz N., Gunn J. E., 1991, ApJ, 377, 365

Kaviraj S. et al., 2007, ApJS, 173, 619

Kaviraj S., Peirani S., Khochfar S., Silk J., Kay S., 2009, MNRAS, 394, 1713

Kaviraj S., Tan K.-M., Ellis R. S., Silk J., 2011, MNRAS, 411, 2148

Kazantzidis S., Zentner A. R., Kravtsov A. V., Bullock J. S., Debattista V. P., 2009, ApJ, 700, 1896

Kereš D., Katz N., Weinberg D. H., Davé R., 2005, MNRAS, 363, 2

Khoperskov S. A., Bertin G., 2015, MNRAS, 451, 2889

Khoperskov A. V., Khoperskov S. A., Zasov A. V., Bizyaev D. V., Khrapov S. S., 2013, MNRAS, 431, 1230

Kim J. H., Peirani S., Kim S., Ann H. B., An S.-H., Yoon S.-J., 2014, ApJ, 789, 90

Kormendy J., 1979, ApJ, 227, 714

Kormendy J., 1982, in Martinet L., Mayor M., eds, Morphology and Dynamics of Galaxies. Geneva Observatory, Sauverny, p. 113

Kormendy J., 1984, ApJ, 286, 116

Kormendy J., 2013, in Falcón-Barroso J., Knapen J. H., eds, Secular Evolution of Galaxies. Cambridge Univ. Press, Cambridge, p. 1

Kormendy J., Bender R., 2012, ApJS, 198, 2

Kormendy J., Kennicutt R. C., 2004, ARA&A, 42, 603

Kostiuk I. P., Sil'chenko O. K., 2015, Balt. Astron., 24, 426

Kregel M., van der Kruit P. C., de Grijs R., 2002, MNRAS, 334, 646

Kuijken K., 1991, ApJ, 376, 467

Kuijken K., Fisher D., Merrifield M. R., 1996, MNRAS, 283, 543

Larsen J. A., Humphreys R. M., 2003, AJ, 125, 1958

López-Corredoira M., Molgó J., 2014, A&A, 567, A106

Lütticke R., Dettmar R. J., Pohlen M., 2000, A&A, 362, 435

MacArthur L. A., Courteau S., Holtzman J. A., 2003, ApJ, 582, 689

Makarov D., Prugniel P., Terekhova N., Courtois H., Vauglin I., 2014, A&A, 570, A13

Martín-Navarro I. et al., 2012, MNRAS, 427, 1102

Martínez-Delgado D. et al., 2010, AJ, 140, 962

Martinez-Valpuesta I., Shlosman I., Heller C., 2006, ApJ, 637, 214

Martin D. C. et al., 2005, ApJ, 619, L1

Mayya Y. D., Carrasco L., Luna A., 2005, ApJ, 628, L33

McMillan P. J., Dehnen W., 2007, MNRAS, 378, 541

Mei S. et al., 2007, ApJ, 655, 144

Méndez-Abreu J., Simonneau E., Aguerri J. A. L., Corsini E. M., 2010, A&A, 521, A71

Michard R., Marchal J., 1993, A&AS, 98, 29

Michard R., Marchal J., 1994, A&AS, 105, 481

Miskolczi A., Bomans D. J., Dettmar R. J., 2011, A&A, 536, A66

Monachesi A. et al., 2019, MNRAS, 485, 2589

Morales G., Martínez-Delgado D., Grebel E. K., Cooper A. P., Javanmardi B., Miskolczi A., 2018, A&A, 614, A143

Mosenkov A. V., Sotnikova N. Y., Reshetnikov V. P., 2010, MNRAS, 401, 559

Mosenkov A. V., Sotnikova N. Y., Reshetnikov V. P., Bizyaev D. V., Kautsch S. J., 2015, MNRAS, 451, 2376

Mosenkov A. et al., 2020, MNRAS, 494, 1751

Navarro J. F., Frenk C. S., White S. D. M., 1996, ApJ, 462, 563

Notni P., Bronkalla W., 1983, in Athanassoula E., ed., Proc. IAU Symp. 100, Internal Kinematics and Dynamics of Galaxies. Kluwer, Dordrecht, p. 67

Ostriker E. C., Binney J. J., 1989, MNRAS, 237, 785

Ostriker J. P., Tremaine S. D., 1975, ApJ, 202, L113

Paladini R., Davies R. D., De Zotti G., 2004, MNRAS, 347, 237

Pfenniger D., Friedli D., 1991, A&A, 252, 75

Pfenniger D., Norman C., 1990, ApJ, 363, 391

Proshina I. S., Kniazev A. Y., Sil'chenko O. K., 2019, AJ, 158, 5

Proshina I., Sil'chenko O., Moiseev A., 2020, A&A, 634, A102

Raha N., Sellwood J. A., James R. A., Kahn F. D., 1991, Nature, 352, 411

Read J. I., Lake G., Agertz O., Debattista V. P., 2008, MNRAS, 389, 1041

Reshetnikov V., Combes F., 1998, A&A, 337, 9

Reshetnikov V., Battaner E., Combes F., Jiménez-Vicente J., 2002, A&A, 382, 513

Reshetnikov V. P., Mosenkov A. V., Moiseev A. V., Kotov S. S., Savchenko S. S., 2016, MNRAS, 461, 4233

Revaz Y., Pfenniger D., 2004, A&A, 425, 67

Rich R. M. et al., 2019, MNRAS, 490, 1539

Rieke G. H., Lebofsky M. J., Thompson R. I., Low F. J., Tokunaga A. T., 1980, ApJ, 238, 24

Roškar R., Debattista V. P., Brooks A. M., Quinn T. R., Brook C. B., Governato F., Dalcanton J. J., Wadsley J., 2010, MNRAS, 408, 783

Sadoun R., Mohayaee R., Colin J., 2014, MNRAS, 442, 160

Sage L. J., Welch G. A., 2006, ApJ, 644, 850

Sanchez-Saavedra M. L., Battaner E., Florido E., 1990, MNRAS, 246, 458

Sancisi R., 1976, A&A, 53, 159

Sandage A., 1961, The Hubble Atlas of Galaxies. Carnegie Institution, Washington

Sandage A., Bedke J., 1994, The Carnegie Atlas of Galaxies. Carnegie Institution, Washington

Schlafly E. F., Finkbeiner D. P., 2011, ApJ, 737, 103

Semczuk M., Lokas E. L., D'Onghia E., Athanassoula E., Debattista V. P., Hernquist L., 2020, preprint (arXiv:2002.07022)

Serra P. et al., 2012, MNRAS, 422, 1835

Sérsic J. L., 1963, Boletin de la Asociacion Argentina de Astronomia La Plata Argentina, 6, 41

Sérsic J. L., 1968, Atlas de Galaxias Australes. Observatorio Astronomico, Cordoba, Argentina

Sharma S., Steinmetz M., 2005, ApJ, 628, 21

Sharma S., Steinmetz M., Bland-Hawthorn J., 2012, ApJ, 750, 107

Shen J., Sellwood J. A., 2006, MNRAS, 370, 2

Shen S., Mo H. J., White S. D. M., Blanton M. R., Kauffmann G., Voges W., Brinkmann J., Csabai I., 2003, MNRAS, 343, 978

Sil'chenko O. K., 2016, Astron. Lett., 42, 163

Sil'chenko O. K., Moiseev A. V., 2006, AJ, 131, 1336

Sil'chenko O. K., Moiseev A. V., Afanasiev V. L., 2009, ApJ, 694, 1550

Sil'chenko O., Kostiuk I., Burenkov A., Parul H., 2018, A&A, 620, L7

Sil'chenko O. K., Moiseev A. V., Egorov O. V., 2019, ApJS, 244, 6

Smirnov A. A., Sotnikova N. Y., 2019, MNRAS, 485, 1900

Smith M. W. L. et al., 2012, ApJ, 748, 123

Sotnikova N. Y., Reshetnikov V. P., Mosenkov A. V., 2012, Astron. Astrophys. Trans., 27, 325

Sparke L. S., Casertano S., 1988, MNRAS, 234, 873

Stevens A. R. H., Lagos C. del P., Contreras S., Croton D. J., Padilla N. D., Schaller M., Schaye J., Theuns T., 2017, MNRAS, 467, 2066

Taylor R., Davies J. I., Auld R., Minchin R. F., 2012, MNRAS, 423, 787

Teeninga P., Moschini U., Trager S. C., Wilkinson M. H., 2015, International Symposium on Mathematical Morphology and Its Applications to Signal and Image Processing. Springer, Cham, p. 157

Teuben P., 1995, in Shaw R. A., Payne H. E., Hayes J. J. E., eds, ASP Conf. Ser. Vol. 77, Astronomical Data Analysis Software and Systems IV. Astron. Soc. Pac., San Francisco, p. 398

Thakar A. R., Ryden B. S., 1996, ApJ, 461, 55

Thakar A. R., Ryden B. S., 1998, ApJ, 506, 93

Thomas P. A. et al., 1998, MNRAS, 296, 1061

Tonry J., Schneider D. P., 1988, AJ, 96, 807

Toomre A., 1983, in Athanassoula E., ed., IAU Symp. 100, Internal Kinematics and Dynamics of Galaxies. Kluwer, Dordrecht, p. 177

Tully R. B., Fisher J. R., 1977, A&A, 500, 105

Tully R. B., Fisher J. R., 1988, Catalog of Nearby Galaxies. Cambridge Univ. Press, Cambridge

Valenzuela O., Rhee G., Klypin A., Governato F., Stinson G., Quinn T., Wadsley J., 2007, ApJ, 657, 773

van den Bergh S., 1976, ApJ, 206, 883

van den Bosch F. C., Abel T., Croft R. A. C., Hernquist L., White S. D. M., 2002, ApJ, 576, 21

van der Kruit P. C., Freeman K. C., 2011, ARA&A, 49, 301

van der Kruit P. C., Searle L., 1981, A&A, 95, 105

van Dokkum P. et al., 2019, ApJ, 883, L32

Vauterin P., Dejonghe H., 1997, MNRAS, 286, 812

Velliscig M. et al., 2015, MNRAS, 453, 721

Vera-Ciro C. A., Sales L. V., Helmi A., Frenk C. S., Navarro J. F., Springel V., Vogelsberger M., White S. D. M., 2011, MNRAS, 416, 1377

Vesperini E., Weinberg M. D., 2000, ApJ, 534, 598

Vogelsberger M. et al., 2014, MNRAS, 444, 1518

Wang Y., Yang X., Mo H. J., Li C., van den Bosch F. C., Fan Z., Chen X., 2008, MNRAS, 385, 1511

Warren M. S., Quinn P. J., Salmon J. K., Zurek W. H., 1992, ApJ, 399, 405

Welch G. A., Sage L. J., 2003, ApJ, 584, 260

Welch G. A., Sage L. J., Young L. M., 2010, ApJ, 725, 100

Wen X.-Q., Wu H., Zhu Y.-N., Lam M. I., Wu C.-J., Wicker J., Zhao Y.-H., 2013, MNRAS, 433, 2946

Wright E. L. et al., 2010, AJ, 140, 1868

Yang X., van den Bosch F. C., Mo H. J., Mao S., Kang X., Weinmann S. M., Guo Y., Jing Y. P., 2006, MNRAS, 369, 1293

Yanny B. et al., 2000, ApJ, 540, 825

York D. G. et al., 2000, AJ, 120, 1579

Yoshida N., Springel V., White S. D. M., Tormen G., 2000, ApJ, 544, L87

Yun M. S., Ho P. T. P., Lo K. Y., 1993, ApJ, 411, L17

Yurin D., Springel V., 2015, MNRAS, 452, 2367

Zasov A. V., Saburova A. S., Khoperskov A. V., Khoperskov S. A., 2017, Phys.-Usp., 60, 3

Zhu Q., Marinacci F., Maji M., Li Y., Springel V., Hernquist L., 2016, MNRAS, 458, 1559

Zibetti S., Ferguson A. M. N., 2004, MNRAS, 352, L6

APPENDIX A: NGC 509

Here, we consider an initially selected 'edge-on' galaxy with a tilted outer structure, NGC 509. In Fig. A1, you can see its deep image which reveals an incredibly tilted halo (or thick disc) with respect to the stellar disc.

However, after a careful investigation, we concluded that NGC 509 cannot be treated as an edge-on galaxy with an inclined bright halo (or thick disc?). The kinematical tilted-ring analysis of the 2D stellar velocity field, provided by the ATLAS-3D survey (Cappellari et al. 2011), reveals that the disc inclination is equal to approximately 65°. It also reveals the bar-induced non-circular stellar rotation.
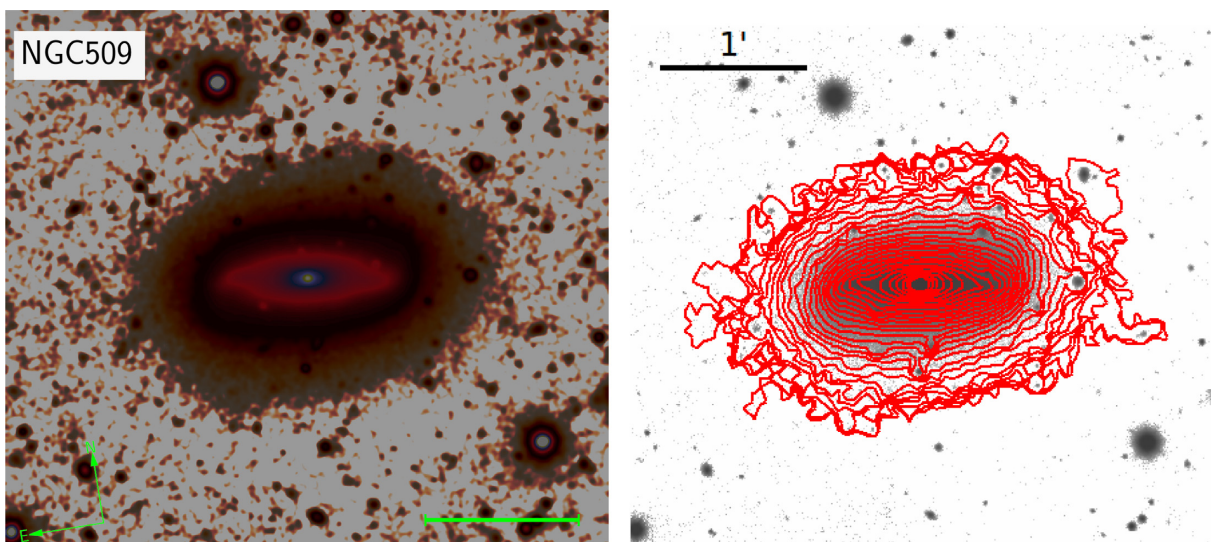
Figure A1. Stacked Legacy *grz* image for NGC 509 (left plot) and its superimposed isophotes from 20 to 26 mag arcsec^{-2} (right plot).
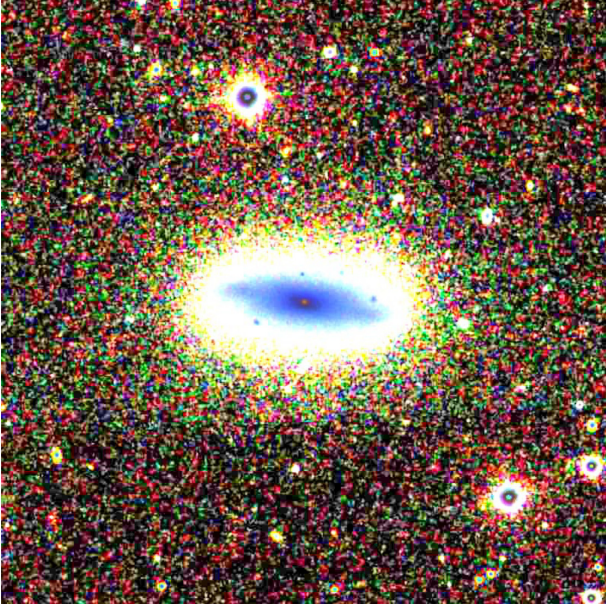
Figure A2. The contrast-enhanced snapshot image of NGC 509 based on a SDSS colour image.

The blue feature inside the thin inner disc is probably a bar with blue ansae (see Fig. A2). The true disc is seen beyond the bar, it has a photometrically implied orientation of the line of nodes equal to PA = 97°. If we inspect Fig. A3, where we compare the photometric and kinematical major axes in the centre of NGC 509 with the line of nodes for the outer disc (general plane of the galaxy), we can see that the photometric and kinematical major
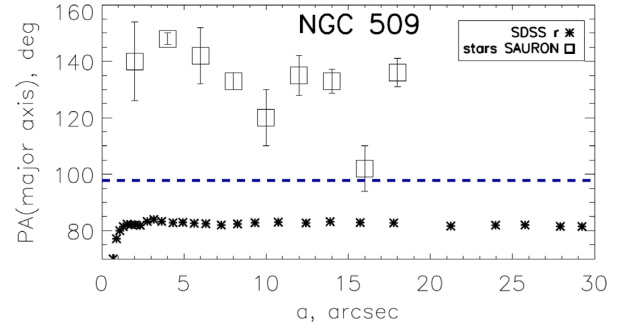

Figure A3. The results of the tilted-ring analysis for the SAURON stellar velocity field. The orientation of the kinematical major axis is shown by large squares in comparison with the photometric major axis (asterisks, the SDSS *r* band) and with the outer disc line of nodes (blue dashed line).

axes deviate from the line of nodes in different directions. Such a behaviour is predicted by dynamical simulations of star rotation in a non-axisymmetrical potential: the zero-velocity line, while in an axisymmetrical potential, traces the isophote minor axis, but in the bar-dominated potential it turns along the bar (Vauterin & Dejonghe 1997). This means that the zero-velocity line tends to align with the major axis of the bar (photometric major axis of NGC 509), whereas the kinematical major axis looks oriented perpendicular to the bar major axis. This proves that NGC 509 is indeed a barred galaxy with a rather moderate inclination to the line of sight. Therefore its 'tilted' outer structure is in fact a consequence of the galaxy inclination and the bar orientation with respect to the observer.
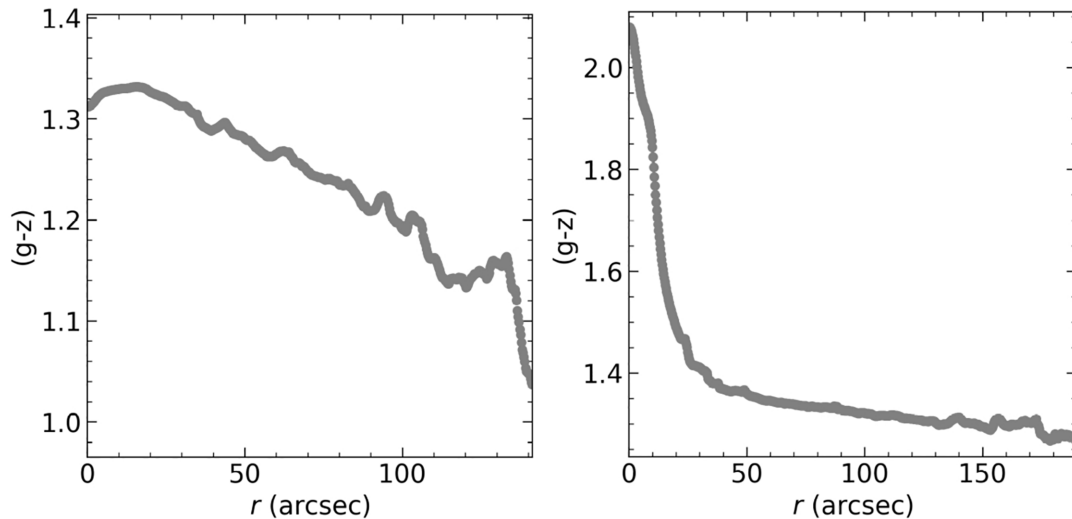
APPENDIX B: RADIAL COLOUR PROFILES

Figure B1. Radial colour profiles for NGC 4452 (the left hand plot) and NGC 4469 (right plot), which were created based on the Legacy data .

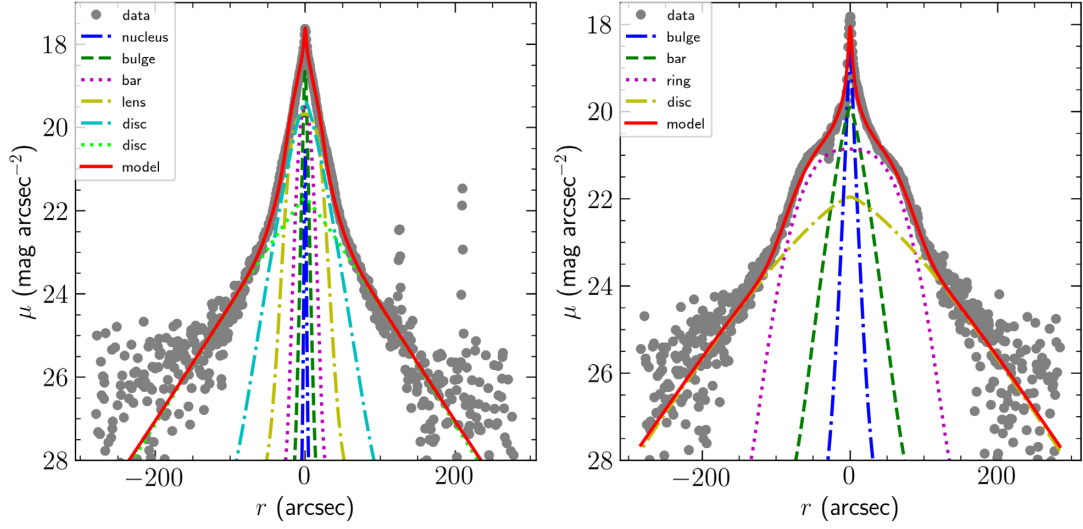## APPENDIX C: MAJOR-AXIS PROFILES

Figure C1. Photometric cuts along the major axes of the outer discs for NGC 4452 (left plot) and NGC 4469 (right plot) with the superimposed corresponding decomposition models.

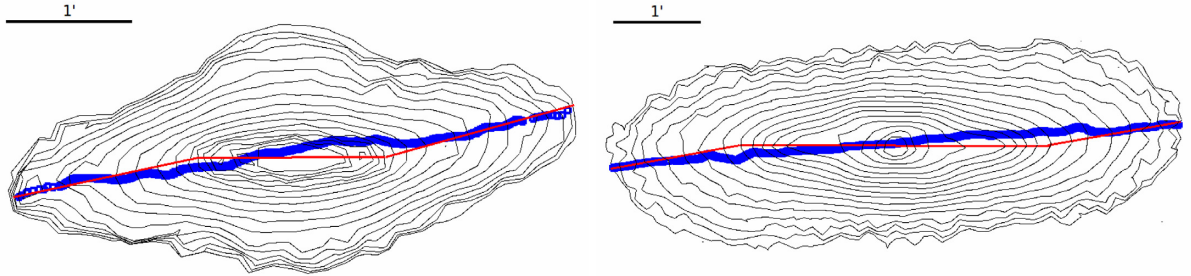## APPENDIX D: CHARACTERISTICS OF WARPS

Figure D1. Contour maps for NGC 4452 (left plot) and NGC 4469 (right plot). The red lines correspond to the best fits of the centre lines, based on all isophotes, with piecewise linear functions. The outermost isophote in each plot is of 25.5 mag arcsec^{-2}, with the blue line, which represents the centre line of this isophote.

APPENDIX E: SIMULATIONS OF GALAXIES WITH BARS

Here, we briefly describe the details of our simulations which we use in Section 4. To create the initial equilibrium state, we used a script for constructing the equilibrium multicomponent model of a galaxy `mkgalaxy` (McMillan & Dehnen 2007) from the toolbox for *N*-body simulation `NEMO` (Teuben 1995). We considered two models; each model consisted of an exponential disc isothermal in the vertical direction

$$\rho(R, z) = \frac{M_\mathrm{d}}{8\pi h^2 z_0} \exp(-R/h) \operatorname{sech}^2(z/(2z_0)), \tag{E1}$$

and a dark halo of NWF profile (Navarro, Frenk & White 1996) represented by a set of particles with $N_\mathrm{d} = 4 \times 10^6$ and $N_\mathrm{h} = 4.5 \times 10^6$, respectively. The radial velocity dispersion profile of the disc was chosen to obey an exponential law, $\sigma_R = \sigma_0 \times \exp(-R/2h)$, where the σ_0 value follows from the condition on the Toomre value parameter at $R = 2h$, $Q(2h) = Q_0$. First model (Model 1) considered has a relatively thin, cool (in a dynamical sense), and rather massive initial disc with $z_0 = 0.025\,h$, $Q_0 = 1.2$ and $M_\mathrm{halo}(R < 4h)/M_\mathrm{d} = 1$. The second one (Model 2) has a thicker, hotter, and lighter disc with $z_0 = 0.05\,h$, $Q_0 = 2.0$ and $M_\mathrm{halo}(R < 4h)/M_\mathrm{d} = 1.5$. The simulations were carried out in a self-consistent manner, that is, both the disc and the halo were allowed to evolve under the influence of their mutual gravitational field. The

equations of motions were solved by the fast numerical integrator `gyrfalcON` (Dehnen 2002) for about 6 Gyr with an adaptive time-step with the maximal value of about 2×10^{-3} Gyr. Both models developed a strong bar that have a B/PS bulge appearance if seen edge-on. Model images presented in Fig. 12 are obtained by rotations of the bar major axis and the disc plane, and integrating the density of the luminous matter along the line of sight. In Fig. E1, we present the results of the IRAF/ELLIPSE fitting for NGC 3869 and the Model 1 image. We can observe a change of the position angle in the inner region, where the B/PS bulge dominates ($B_4 < 0$), by approximately 7° for NGC 3869 and 10° for Model 1. Also, note similar behaviours of all light distributions for both galaxies.
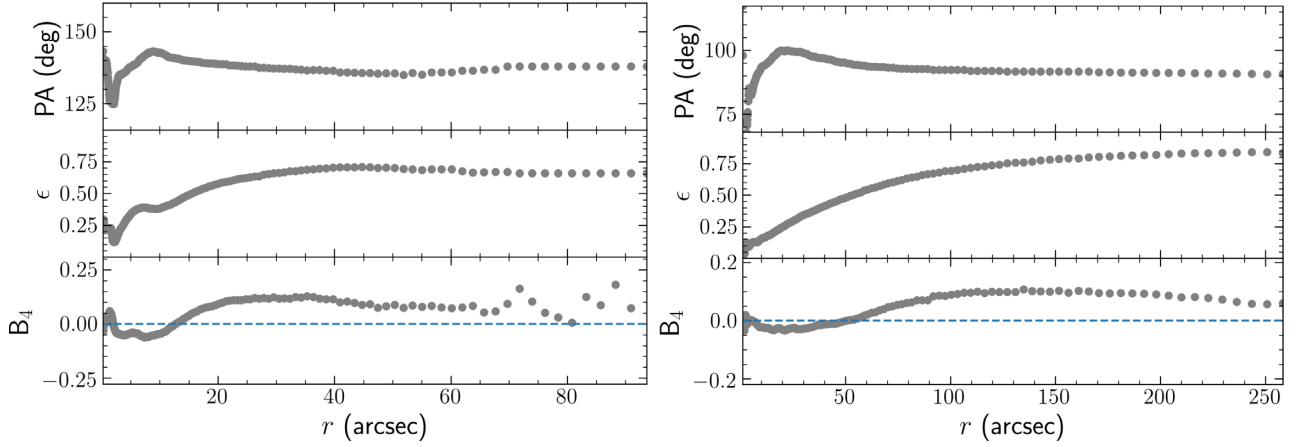

Figure E1. Results of the IRAF/ELLIPSE fitting for NGC 3869 (left plot) and the Model 1 (right plot).

This paper has been typeset from a TEX/LATEX file prepared by the author.